Acta Pharmaceutica Sinica B 2025;15(2):973−990

Chinese Pharmaceutical Association
Institute of Materia Medica, Chinese Academy of Medical Sciences

Acta Pharmaceutica Sinica B

www.elsevier.com/locate/apsb
www.sciencedirect.com

ORIGINAL ARTICLE

FLZ attenuates Parkinson's disease pathological damage by increasing glycoursodeoxycholic acid production *via* down-regulating *Clostridium innocuum*

Meiyu Shang, Jingwen Ning, Caixia Zang, Jingwei Ma, Yang Yang, Yueqi Jiang, Qiuzhu Chen, Yirong Dong, Jinrong Wang, Fangfang Li, Xiuqi Bao*, Dan Zhang*

State Key Laboratory of Bioactive Substrate and Function of Natural Medicine, Institute of Materia Medica, Chinese Academy of Medical Sciences and Peking Union Medical College, Beijing 100050, China

Received 15 May 2024; received in revised form 8 July 2024; accepted 26 July 2024

KEY WORDS

Parkinson's disease;
FLZ;
Glycoursodeoxycholic acid;
Clostridium innocuum;
Gut−brain axis;
Microbiota dysbiosis;
Microbial metabolites;
Neuroinflammation

Abstract Increasing evidence shows that the early lesions of Parkinson's disease (PD) originate from gut, and correction of microbiota dysbiosis is a promising therapy for PD. FLZ is a neuroprotective agent on PD, which has been validated capable of alleviating microbiota dysbiosis in PD mice. However, the detailed mechanisms still need elucidated. Through metabolomics and 16S rRNA analysis, we identified glycoursodeoxycholic acid (GUDCA) was the most affected differential microbial metabolite by FLZ treatment, which was specially and negatively regulated by *Clostridium innocuum*, a differential microbiota with the strongest correlation to GUDCA production, through inhibiting bile salt hydrolase (BSH) enzyme. The protection of GUDCA on colon and brain were also clarified in PD models, showing that it could activate Nrf2 pathway, further validating that FLZ protected dopaminergic neurons through promoting GUDCA production. Our study uncovered that FLZ improved PD through microbiota−gut−brain axis, and also gave insights into modulation of microbial metabolites may serve as an important strategy for treating PD.

*Corresponding authors.
E-mail addresses: baoxiuqi@imm.ac.cn (Xiuqi Bao), danzhang@imm.ac.cn (Dan Zhang).

Peer review under the responsibility of Chinese Pharmaceutical Association and Institute of Materia Medica, Chinese Academy of Medical Sciences.

https://doi.org/10.1016/j.apsb.2024.10.011

1. Introduction

Parkinson's disease (PD) is an age related neurodegenerative disease affecting over 6 million patients worldwide[1]. Previous studies indicated that the degeneration of the central nigrostriatal system triggered the onset of PD. However, in recent years, accumulating evidence has shown that up to 30% patients with PD experience gastrointestinal (GI) symptoms before the central nervous system (CNS) impairment and motor dysfunction[2]. These symptoms involve decreased frequency of bowel movement, increased gut inflammation and gut barrier permeability[3]. Moreover, it has been confirmed that α-synuclein aggregation exists in the enteric nervous system at the early stage of PD and misfolded α-synuclein can spread from the vagus nerve in the GI tract to the brain[4], demonstrating that the early lesions of PD may originate from the gut. Clinical studies have revealed that microbiota dysbiosis exists in PD patients, evidenced by a decreased abundance of probiotics and an increased abundance of harmful bacteria, which damage the enteric barrier and lead to gut inflammation[5]. These findings suggest that microbiota dysbiosis leads to gut dysfunction as the key event in the pathogenesis of PD. Gut microbiota communicates with the host mainly through microbial metabolites, including short chain fatty acids (SCFAs), γ-aminobutyric acid, dopamine, tryptophan and secondary bile acids, etc. These microbial metabolites can enter the circulation and alter intestinal, peripheral and CNS inflammation, finally affecting the trafficking of immune cells into the brain. Certain protective metabolites of bacteria, including SCFAs and bile acids, are downregulated in PD. In contrast, noxious metabolites, such as amino acid derivates or trimethylamine-oxide are upregulated[6], indicating that disruption of metabolism accelerates the disease progression.

Correcting microbiota dysbiosis and gut dysfunction are promising for early PD treatments. A recent study revealed that transplantation of healthy mice fecal microbiota to PD mice could attenuate intestinal inflammation and prevent barrier impairment[7]. Resveratrol and curcumin, which have been recognized to be capable of correcting gut microbiota dysbiosis, were proven to exert neuroprotective effects on PD partly through alleviating gut dysfunction[8]. FLZ is a novel neuroprotective agent derived from squamosamide (Supporting Information Fig. S1A), showing significant neuroprotective effects on several PD models, including 1-methyl-4-phenyl-1,2,3,6-tetrahydropyridine (MPTP) induced subacute PD mouse model[9], 6-hydroxydopamine (6-OHDA) induced subacute PD rat model[10], MPTP combined with probenecid induced chronic PD mouse model[11], and α-synuclein transgenic mouse model[12]. Previous mechanistic studies have revealed that FLZ is a multitarget drug, which not only alleviates dopaminergic neuron degeneration through activating the protein kinase B/mammalian target of the rapamycin pathway[9], but also suppresses microglia mediated neuroinflammation by inhibiting Src tyrosine kinase[13]. FLZ is well tolerated by healthy subjects, with favorable safety profile in phase I clinical study, and now is prepared to enter phase II clinical study. Pharmacokinetic studies indicated that the absorption and metabolism of FLZ were dependent on lanosterol 14α-demethylase produced by gut microbiota[14]. FLZ could also improve the composition and abundance of gut microbiota, thereby alleviating neuroinflammation and motor dysfunction in PD mouse model[15]. However, the mechanism by which FLZ affects the gut microbiome to regulate microbial metabolites and improve motor functions in PD remains incompletely elucidated.

In the present study, we aimed to explore specific gut microbiota and microbial metabolites contributing to the therapeutic effects of FLZ on PD. We first employed an exhaustive untargeted metabolomics method and identified a key differential metabolite glycoursodeoxycholic acid (GUDCA) that was markedly affected by the FLZ treatment. Then, 16S rRNA analysis showed that FLZ increased GUDCA production by inhibiting the bile salt hydrolase (BSH) enzyme in *Clostridium innocuum*, a differential microbiota with the strongest correlation with GUDCA. Finally, we clarified the neuroprotective effects of GUDCA in both *in vitro* and *in vivo* PD models. Our present study uncovered the detailed mechanisms by which FLZ improved PD through the microbiota−gut−brain axis, and highlighted that targeting gut microbiota and its metabolites might serve as an important strategy for treating PD.

2. Material and methods

2.1. Animals and PD mouse model development

2.1.1. Animals

Male C57BL/6J mice weighing 22−25 g were obtained from Beijing HFK Bioscience Co., Ltd. (Beijing, China). Mice were kept under standard conditions (temperature 22 ± 2 °C and humidity 50%−60% on a 12 h light/dark cycle) with free to food and water available. They were allowed to acclimate to environment for three days before experimentation. All the experimental procedures were performed in accordance with the guidelines of the Beijing Municipal Ethics Committee for the care and use of laboratory animals, and were approved by the Animal Care & Welfare Committee, Institute of Materia Medica, CAMS &PUMC (Nos. 00005071 and 00004323).

2.1.2. Development of 1-methyl-4-phenyl-1,2,3,6-tetrahydropyridine/probenecid (MPTP/p)-induced PD mouse model and treatments

Chronic PD mouse model was achieved by injection the combination of MPTP (Sigma−Aldrich, USA) and probenecid (Sigma−Aldrich, USA). Briefly, mice were intraperitoneally injected with probenecid (250 mg/kg, dissolved in DMSO) 30 min prior to subcutaneously injection of MPTP hydrochloride (25 mg/kg, dissolved in saline) to induce parkinsonian symptoms, while Control mice were injected with vehicles. These mice were received a total of 10 injections of MPTP in combination with probenecid. The 10 injections were given at an interval of 3.5 days for a 5-week schedule. The mice were then orally administrated with FLZ (prepared by Institute of Materia Medica, Chinese Academy of Medical Sciences and Peking Union Medical College with 99% purity) 75 mg/kg, suspended in 0.5% CM-cellulose, sodium salt (CMC-Na), once a day for 8 weeks, Control mice and MPTP/p mice were treated with 0.5% CMC-Na. GI functional evaluation and behavioral tests were performed at 9th week and 13th week, respectively. The procedure of mice treatment is shown in Fig. S1B.

2.1.3. Development of rotenone-induced PD mouse model and treatments

Mice were orally administrated with freshly prepared rotenone (Sigma−Aldrich, USA) solution (30 mg/kg, suspended in 0.5% CMC-Na) once a day for 4 weeks (week 1−4), and Control mice were treated with 0.5% CMC-Na. From 3rd week, GUDCA (Targetmol, China) 50 mg/kg and FLZ 75 mg/kg were orally administrated to rotenone-challenged mice once a day for 4 weeks,

respectively. GI functional evaluation and behavioral tests were performed at 6th week after the last GUDCA and FLZ treatments.

2.2. T3 UPLC conditions and ESI-QTRAP-MS/MS for non-targeted metabolomics

At the end of the 13th week after the last FLZ treatment, the feces, urine, midbrain and blood samples were collected from 6 mice in each group for non-targeted metabolomics study. All the samples were processed with grinding and centrifugation. And then, a 200 μL aliquots of supernatant obtained from the pretreated samples were transferred into vials and undergoing the LC−MS analysis. The sample extracts were analyzed using an LC−ESI-MS/MS system (UPLC, ExionLC AD, https://sciex.com.cn/; MS, QTRAP® System, https://sciex.com/). The analytical conditions were as follows, UPLC: column, Waters ACQUITY UPLC HSS T3 C18 (1.8 μm, 2.1 mm × 100 mm); column temperature, 40 °C; flow rate, 0.4 mL/min; injection volume, 2 μL; solvent system, water (0.1% formic acid):acetonitrile (0.1% formic acid); gradient program, 95:5 *v*/*v* at 0 min, 10:90 *v*/*v* at 11.0 min, 10:90 *v*/*v* at 12.0 min, 95:5 *v*/*v* at 12.1 min, 95:5 *v*/*v* at 14.0 min. LIT and triple quadrupole (QQQ) scans were acquired on a triple quadrupole-linear ion trap mass spectrometer (QTRAP), QTRAP® LC−MS/MS System, equipped with an ESI Turbo Ion-Spray interface, operating in positive and negative ion mode and controlled by Analyst 1.6.3 software (Sciex). The ESI source operation parameters were as follows: source temperature 500 °C; ion spray voltage (IS) 5500 V (positive), −4500 V (negative); ion source gas I (GSI), gas II (GSII) and curtain gas (CUR) were set at 55, 60, and 25.0 psi, respectively; the collision gas (CAD) was high. Instrument tuning and mass calibration were performed with 10 and 100 μmol/L polypropylene glycol solutions in QQQ and LIT modes, respectively. A specific set of MRM transitions was monitored for each period according to the metabolites eluted within this period.

2.3. 16S rRNA gene sequencing

Four mice were randomly chosen from each group at 13th week to collect feces for 16S rRNA sequencing. All samples were then frozen instantly and stored at −80 °C prior to analyzed. Total genome DNA from stool sample was extracted using CTAB/SDS method. DNA concentration and purity was monitored on 1% agarose gels, and was diluted to 1 ng/μL using sterile water. 16S rRNA/18S rRNA/ITS genes of distinct regions (16S V4/16S V3/16S V3−V4/16S V4−V5, 18S V4/18S V9, ITS1/ITS2, Arc V4) were amplified using specific primer (*e.g.*, 16S V4: 515F-806R, 18S V4: 528F-706R, 18S V9: 1380F-1510R, etc.) with the barcode. All PCR reactions were carried out with 15 μL of Phusion® High-Fidelity PCR Master Mix (New England Biolabs), 0.2 μmol/L of forward and reverse primers, and about 10 ng template DNA. Thermal cycling consisted of initial denaturation at 98 °C for 1 min, followed by 30 cycles of denaturation at 98 °C for 10 s, annealing at 50 °C for 30 s, elongation at 72 °C for 30 s, and finally 72 °C for 5 min. Mix the same volume of 1 × loading buffer (contained SYB green) with the PCR products and subjected to electrophoresis on 2% agarose gel for detection. PCR products was mixed in equinity ratios. Then, the mixture of PCR products was purified with Qiagen Gel Extraction Kit (Qiagen, Germany). Sequencing libraries were generated using TruSeq® DNA PCR-Free Sample Preparation Kit (Illumina, USA) following manufacturer's recommendations and index codes were added. The library quality was assessed on the Qubit@ 2.0 Fluorometer (Thermo Scientific) and Agilent Bioanalyzer 2100 system. At last, the library was sequenced on an Illumina NovaSeq platform and 250 bp paired-end reads were generated.

2.4. Bioinformatics analysis

Paired-end reads were assigned to samples based on their unique barcode and truncated by cutting off the barcode and primer sequence, and merged using FLASH (V1.2.7, http://ccb.jhu.edu/software/FLASH/)[16], a very fast and accurate analysis tool, which was designed to merge paired-end reads when at least some of the reads overlap the read generated from the opposite end of the same DNA fragment, and the splicing sequences were called raw tags. Quality filtering on the raw tags were performed under specific filtering conditions to obtain the high-quality clean tags[17] according to the QIIME (V1.9.1, http://qiime.org/scripts/split_libraries_fastq.html)[18] quality controlled process. The tags were compared with the reference database (Silva database, https://www.arbsilva.de/) using UCHIME algorithm (UCHIME Algorithm, http://www.drive5.com/usearch/manual/uchime_algo.html)[19] to detect chimera sequences, and then the chimera sequences were removed[20] and the effective tags were finally obtained.

The mass spectrum data was processed using Analyst 1.6.3 software. All data analysis was based on the self-built MWDB database (MetwareBiotechnology Co., Ltd., Wuhan, China). The principal component analysis (PCA) and latent structures-discriminant analysis (OPLS-DA) were generated using R package MetaboAnalystR (v1.0.1). Significantly regulated metabolites between groups were determined by Variable Importance in Projection (VIP) value and Fold Change (FC) value, where VIP$\geq$1 and FC $\geq$ 2 or FC $\leq$ 0.5 were considered to be significant. The differential metabolites were annotated by KEGG compound database (http://www.kegg.jp/kegg/compound/) and then mapped to the KEGG pathway database (http://www.kegg.jp/kegg/pathway.html). The Receiver Operating Characteristic curve (ROC) analysis was performed in (https://www.metaboanalyst.ca/) using 10 increase and 10 decrease metabolites with the largest absolute $\log_2$ (Fold change) value in the experimental groups (Control, MPTP/p and MPTP/p+FLZ). The area under the curve (AUC) was calculated. The metabolites were considered as biomarkers if their AUC values were more than 0.7.

2.5. Motor behavior evaluations

2.5.1. The rotarod test

The rotarod test was performed as described previously[11]. Briefly, mice were positioned on the rod of rotarod apparatus (Ugo basile, Germany) and then tested on the revolving rod at the speed of 25 rpm for up to 120 s. The rotarod automatically recorded the time that the animals first fell off the rod, which designated as latency, and the time of latency was recorded.

2.5.2. The pole test

The pole climber (Institute of Materia Medica, Chinese Academy of Medical Sciences) includes a 50 cm wooden pole (3 cm in diameter) and a wooden ball. The base of pole was positioned in the home cage and the wooden ball was fixed on top of the pole to prevent mice from sitting on the top and to help position the mice on the pole. The performance of mice climbing down the pole was scored from 0 to 5 by a scale of 0.5[11]. The mice were pretrained before experiment and then scored the performance of each mouse.

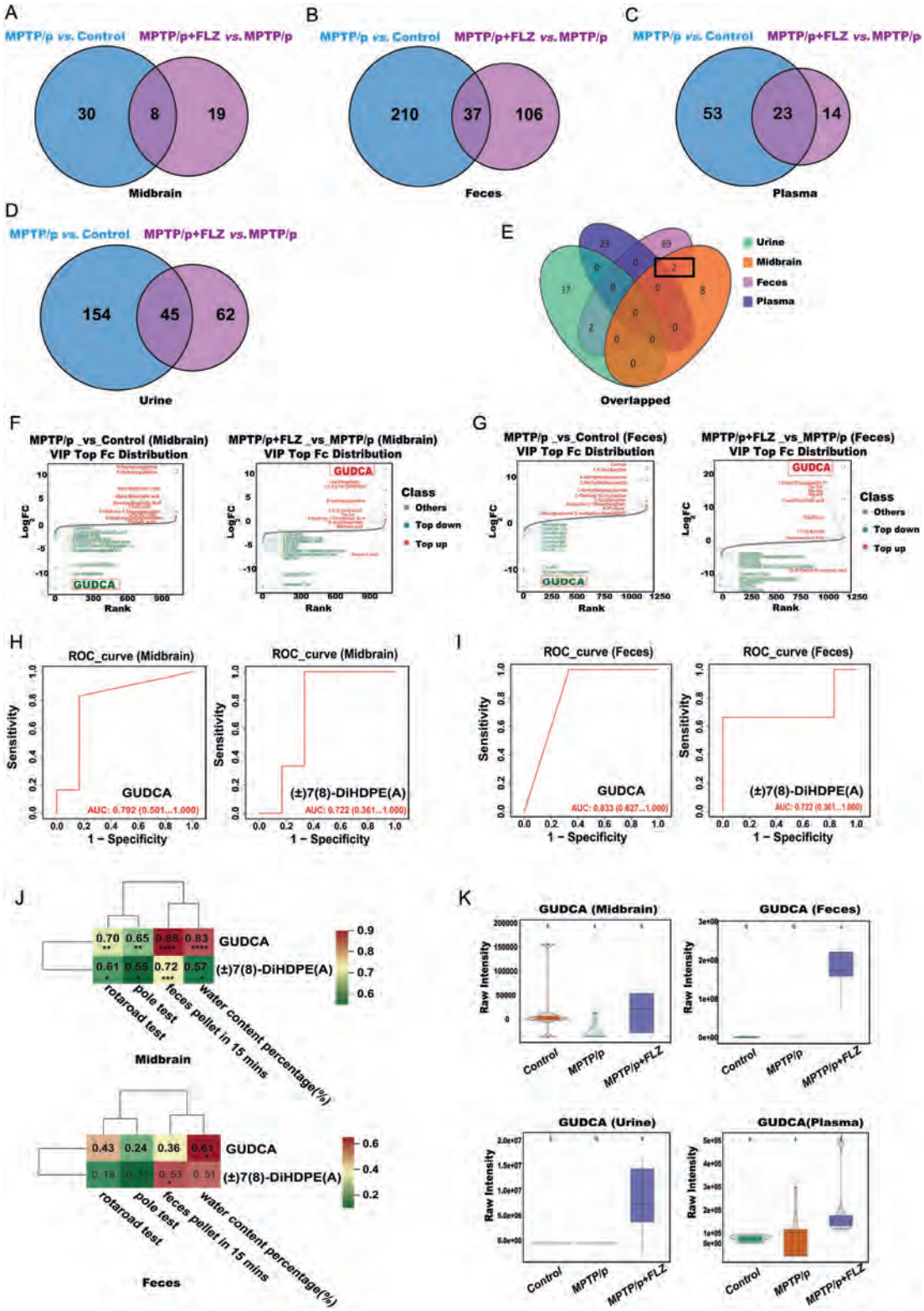

Figure 1 The metabolic profiles of midbrain, fecal, urine and plasma in PD mice treated with FLZ. The MPTP/p-induced PD mice were treated with FLZ for 8 weeks, and then the midbrain, fecal, urine and plasma were collected at 13th week and subjected to untargeted metabolomics analysis. (A) The Venn plot of the midbrain. (B) The Venn plot of the feces. (C) The Venn plot of the plasma. (D) The Venn plot of the urine. (E) The overlapped differential metabolites shown in the Venn plot. (F) The TOP 20 metabolites FC distribution in the midbrain. (G) The TOP 20 metabolites FC distribution in the feces. (H) The ROC curve of GUDCA and (±)7(8)-DiHDPE(A) in the midbrain. (I) The ROC curve of GUDCA and (±)7(8)-DiHDPE(A) in the feces. (J) The correlation heatmaps of GUDCA and (±)7(8)-DiHDPE(A) with PD pathological indexes. (K) The concentrations of GUDCA in the midbrain, feces, urine and plasma. For metabolomics analysis, $n = 6$ in each group. Spearman analysis, $^{*}P < 0.05$, $^{**}P < 0.01$, $^{***}P < 0.001$.

2.5.3. Balance beam walking test

The balance beam (Institute of Materia Medica, Chinese Academy of Medical Sciences) is a custom-built wooden bar (100 cm length × 6 cm width), placed 50 cm above the floor, with one end placed in a dark escape home cage. Testing was performed across three consecutive days. During the first two days, mice were habituated to the escape cage for 2 min, then placed at the starting point and trained to cross the balance beam to reach the escape cage three times. On the third day, mice were placed individually at the starting point and allowed to cross the balance beam. The average time for mice to cross the beam and the number of foot slips on the testing day were analyzed.

2.6. Fecal pellets output of PD mice

All the mice were forced to fast for 12 h, and then each mouse was free to eat for 2 h. Each mouse was arranged in a clean plastic cage and the gut motor function was evaluated by the number of fecal pellets collected at 5 min intervals for a 15 or 20 min period. Next, they stayed in the cages for another 1 h. Fecal pellets were collected and placed in sealed tubes. Subsequently, the numbers of fecal pellets were counted. The feces were weighed to get the wet weight, and dried at 65 °C for 24 h to obtain the dry weight. The water content was calculated according to the difference between the wet and dry fecal pellets weight.

2.7. Immunohistochemical analysis

In rotenone-induced PD mouse model experiment, mice were anesthetized with pentobarbital and perfused transcardially with saline and then with cold 4% paraformaldehyde in 0.1 mol/L phosphate buffer (pH 7.4) at the end of the 6th week. Brains were then removed and sectioned to 40 μm sections at the same position. Coronal sections through the substantia nigra were processed for tyrosine kinase (TH) immunohistochemistry as previously described[12]. Briefly, sections were incubated with rabbit polyclonal TH antibody (1:500, Abcam, CA, USA) and then incubated with the biotinylated secondary antibody and subsequently with avidin-peroxidase. Finally, the labeling was visualized with 0.05% 3,3′-diaminobenzidine (DAB). Images were captured by upright microscope (Nikon E600, Japan). The number of TH-positive cells was calculated by counting the number of TH-positive cells in the substantia nigra pars compacta by using ImageJ software.

2.8. Double immunofluorescence staining

For double immunofluorescence staining of TH and cleaved-caspase3 in the experiment of rotenone-induced PD mouse model, the brain sections were deparaffinized in xylene, hydrated in graded ethanol solutions, and then they were incubated with antigen retrieval buffer and heated to induce antigen retrieval. The sections were incubated with 3% H_2O_2 and goat serum to block endogenous peroxidases and antigens, respectively. The protocol of double immunofluorescence staining involves two rounds of staining. Each round comprises incubation with primary antibodies of rabbit polyclonal TH (1:800, Servicebio, China) and rabbit polyclonal cleaved-caspase3 (1:3000, CST, USA), respectively at 4 °C overnight. Then the sections were incubated with horseradish peroxidase conjugated secondary antibody for 20 min (1:1000, Beijing Zhiyi Intellectual Property Agency, China). After washing, they were incubated with Opal 520 Fluorophore (1:100, Akoya Biosciences) and Opal 620 Fluorophore (1:100, Akoya Biosciences) for 10 min. Images were obtained by a scanner (3Dhistech, Hungary). The integrity intensity of immunofluorescence was calculated using Image J 6.0 software.

2.9. Enzyme-linked immunosorbent assay (ELISA)

In the experiment of rotenone-induced PD mouse model, blood was collected from eyeballs of mice after sacrificed by anesthesia at the end of the 6th week. This operation fully complied with animal ethical requirements. The serum supernatant was collected after centrifugation. The lipopolysaccharides (LPS) endotoxin and tumor necrosis factor-α (TNF-α) in serum of mice were measured by LPS ELISA kit (Henghuibio Co., Ltd., Beijing, China) and TNF-α ELISA kit (Dakewe Biotech Co., Ltd., Shenzhen, China), respectively. All the experimental procedures were performed following the instructions recommended by the manufacturer. The cytokine concentrations were calculated by standard protein concentration.

2.10. Cell culture and treatments

SH-SY5Y cells were purchased from the Cell Culture Center at the Institute of Basic Medical Sciences, Chinese Academy of Medical Sciences and Peking Union Medical College. The cells were grown in Dulbecco's modified Eagle's medium (DMEM, Solarbio, China), supplemented with 10% fetal bovine serum (Sijiqing, China), 100 U/mL penicillin, and 100 μg/mL streptomycin, and were kept at 37 °C in a humidified 5% CO_2 air incubator. For cell viability assay and morphological observation, the cells were seeded in 96-well culture plates at a density of 8×10^3 cells/well. For immunocytochemical staining, the cells were plated in 24-well culture plates at a density of 3×10^4 cells/well. The cells were incubated with GUDCA at the concentration of 1 μmol/L, and challenged with 20 μmol/L rotenone for 24 h.

2.11. Cell viability assay and morphological observation

Cell viability was assessed by the CCK-8 assay. The cells were incubated with 10 μL of CCK-8 solution (meilunbio, Dalian,

Table 1 Comparisons of GUDCA and (±)7(8)-DiHDPE(A) in midbrain and feces.

The metabolic profiling	The overlapped metabolite	MPTP/p *vs.* Control				MPTP/p+FLZ *vs.* MPTP/p			
		P value	Fold change	VIP score	Trend	*P* value	Fold change	VIP score	Trend
Midbrain	GUDCA	0.13	0.14	2.05	Down	0.08	7.05	1.42	Up
	(±)7(8)-DiHDPE(A)	0.07	0.41	2.01	Down	0.08	2.50	2.12	Up
Feces	GUDCA	0.05	5.21E-06	1.81	Down	0.0009	1.95E+07	3.09	Up
	(±)7(8)-DiHDPE(A)	0.16	0.47	1.68	Down	0.07	2.49	2.12	Up

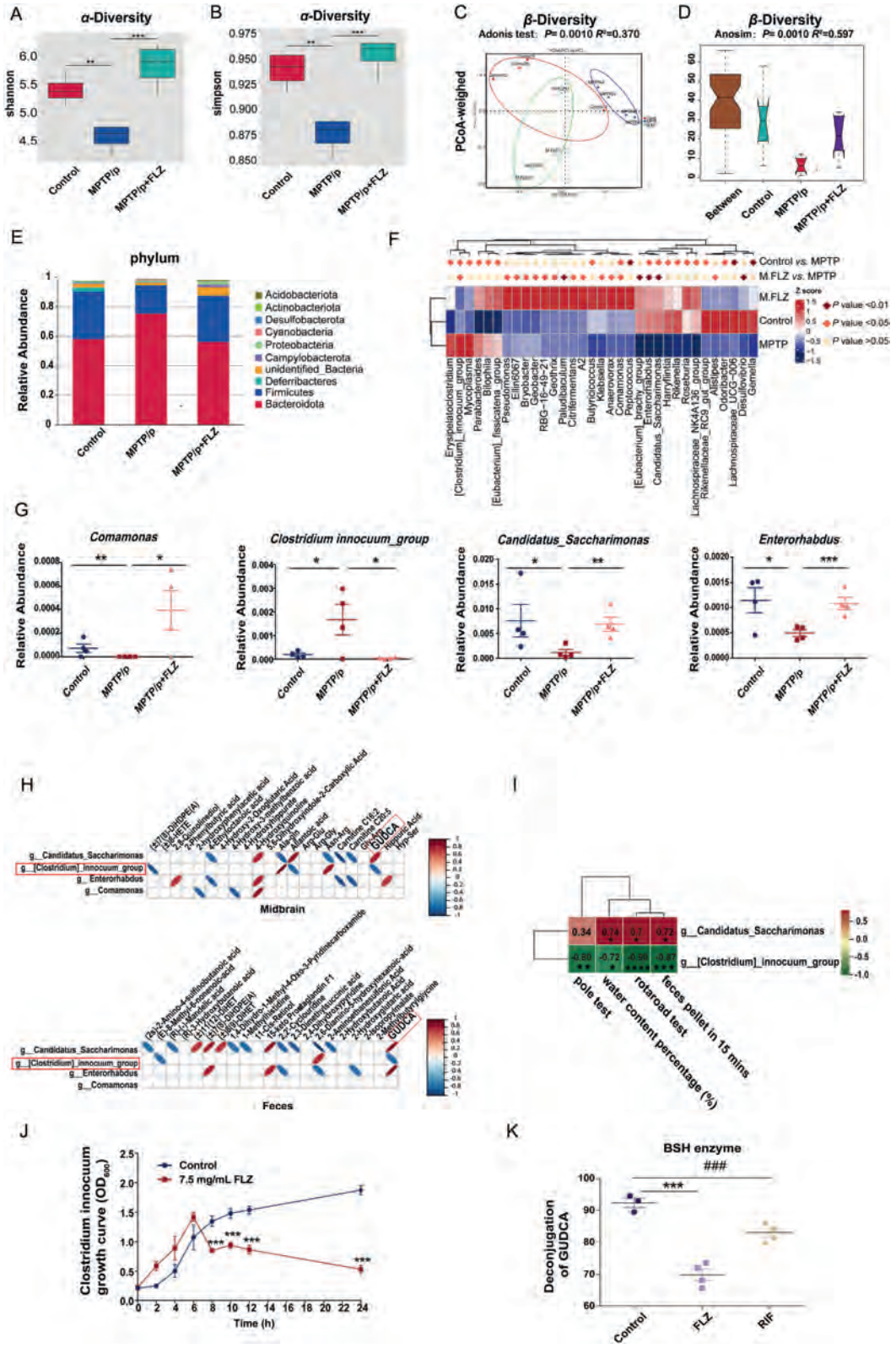

Figure 2 FLZ promoted GUDCA production through inhibiting BSH enzyme in *Clostridium innocuum*. The MPTP/p-induced PD mice were treated with FLZ for 8 weeks, and then the feces were collected at 13th week and subjected to 16S rRNA analysis. (A) Analysis of alpha diversity of gut microbiota based on Shannon analysis. (B) Analysis of alpha diversity of gut microbiota based on Simpson analysis. (C) Analysis of beta diversity based on PCoA weighted UniFrac Adonis analysis. (D) Analysis of Beta diversity based on ANOISM analysis in different groups. (E) Bacterial taxonomic profiling at the phylum levels of gut microbiota in different groups. (F) The metastat analysis at the genus levels of gut microbiota in different groups. (G) The relative abundance of *Comamonas*, *Clostridium innocuum*, *Candidatus Saccharimonas* and

China) for 2 h at 37 °C, and the optical density (OD) was measured using a Microplate Reader (Thermo, Waltham, MA, USA) at a wavelength of 450 nm. The cell viability was expressed as a percentage of the OD value of the Control group. The morphological changes of SH-SY5Y cells in different groups were observed using a phase-contrast microscope (Olympus, Tokyo, Japan).

2.12. Immunofluorescence staining

The cell culture media was removed and the cells were fixed in 4% paraformaldehyde for 30 min at room temperature and washed three times with PBS. The cells were permeabilized in 0.1% TritonX-100 (Sigma−Aldrich, USA) for 10 min and blocked in 3% goat serum for 2 h at room temperature. After an overnight incubation with the anti-nuclear factor erythroid 2-related factor 2 (Nrf2) antibody (Abcam, USA) at 4 °C, the cells were washed three times with 1 × PBS and then incubated with secondary antibody (1:200 dilution, Abcam, USA) for 2 h at room temperature. Afterwards, the cells were washed three times with 1 × PBS and stained with 4,6-diamidino-2-phenylindole (DAPI, Gentihold, China) for 5 min at room temperature. Coverslips were examined and photographed under a confocal microscope (Leica, Germany) with a Leica TCS SP8 system.

2.13. Western blot

Cells were collected 24 h after incubating with GUDCA and challenged with rotenone from 4 to 6 independent experiments. The midbrain, striatum and colon were collected from 4 to 6 mice for Western blot at the end of 6th week. Cells or tissues were homogenized in radioimmunoprecipitation assay (RIPA) lysate buffer (Sangon Biotech, China) with protease phosphatase inhibitor (Solarbio, China) and protease inhibitor (Targetmol, China). Nuclear proteins were obtained using the nuclear-cytosol extraction kit (APPLYGEN, China). The total protein concentrations were determined by bicinchoninic acid (BCA) kit (Yeasen, China) to ensure equal sample loading. Following our previous descriptions[21], proteins were separated by SDS−poly-acrylamide gels (10%) and transferred into a 0.45 μm polyvinylidene fluoride membrane (Millipore, USA), which were then blocked with 5% skim milk-TBST (20 mmol/L of Tris-HCl, pH 7.5, and 500 mmol/L of NaCl, 0.1% Tween 20) for 2 h. The membranes were probed with the following antibodies: β-actin (1:10,000), B-cell lymphoma-2 (Bcl2) (1:1000), heme oxygenase-1 (HO-1) (1:1000), Bcl2-associated x (Bax) (1:1000), quinone oxidoreductase 1 (NQO1) (1:1000), cleaved caspase-3 (1:1000), occludin (1:1000) and claudin-1 (1:1000, Abclonal, China), Lamin B1 (1:1000), tyrosine hydroxylase (TH) (1:1000, Cell Signaling Technology, USA); Nrf2 (1:1000), inducible nitric oxide synthase (iNOS) (1:1000) and cyclooxygenase 2 (COX-2) (1:1000, Abcam, USA), overnight at 4 °C; and then these were incubated with horseradish peroxidase (HRP) goat anti-rabbit IgG (1:2000, Abclonal, China) for 2 h at room temperature. The blots were visualized by incubating the membranes with ECL Plus reagents (Yeasen, China) and the images were recorded by LAS-4000 chemiluminescence system (GE Healthcare, USA). The blot densities were assessed by Gel-pro analyzer 4.0.

2.14. Transmission electron microscopy

In the experiment of rotenone-induced PD mouse model, three mice were randomly selected for anesthesia and perfusion with 0.9% saline at the end of 6th week. The frontal cortex, midbrain and colon tissue were cut into pieces of 1 mm^3. Next, the fresh tissue sections were put into a fixing solution for transmission electron microscopy (TEM, Servicebio) at 4 °C for 4 h and then fixed with 1% OsO_4 in 0.1 mol/L PBS for 2 h at room temperature, followed by dehydration with gradient alcohol. Subsequently, the sections were embedded by baking in an oven at 60 °C for 48 h and cut into ultrathin sections (60 nm) with ultramicrotome. Finally, the ultrastructure of tight junction of the brain and colon were observed using a transmission electron microscope (HITACHI, HT7700, Japan).

2.15. Clostridium innocuum culture and treatment

The *Clostridium innocuum* (Sigma, Germany) was anaerobically incubated in Modified Reinforced Clostridial Broth (ATCC Medium 2107, Biofeng, China) at 37 °C for 48 h and sub-cultured twice before the experiment. Following incubation, it was diluted in the cultured broth with the presence or absence of FLZ (7.5 mg/mL) to the concentration of 1×10^9 CFU/mL and the OD value was measured using a Microplate Reader (Thermo, Waltham, MA, USA) at a wavelength of 600 nm for every 2 h.

2.16. Hydrolysis efficiency of GUDCA

Clostridium innocuum was cultured in Modified Reinforced Clostridial Broth with presence or absence of FLZ. Then *Clostridium innocuum* was adjusted to the equivalent concentration in different groups. The *Clostridium innocuum* were prepared in pH 7.4 PBS and staved with sonication. The obtained proteins were quantified into 0.1 mg/mL with 3 mmol/L sodium acetate buffer (pH 5.2), containing protein and bile acids GUDCA (Targetmol, China) or riboflavin (Targetmol, China) in a final volume of 200 μL. After 1 h incubation of the mixtures at 37 °C, the reactions were stopped in ice. Acetonitrile (200 μL) was directly added to the reaction mix. After centrifuging at 14,000 × *g* for 20 min, 5 μL of the supernatant was transferred to an auto sampler vial and subjected to HPLC−MS analysis.

2.17. Statistical analysis

Statistical analysis was conducted using Graphpad 6.02 software. Data are presented as the mean ± standard error of mean (SEM).

Enterorhabdus. (H) The ellipse heatmap of spearman correlation analysis between differential metabolites and differential gut microbiota. Spearman analysis, $^{*}P < 0.05$, $^{**}P < 0.01$, $^{***}P < 0.001$. (I) Heatmap of pearson correlation between pathological indexes and differential gut microbiota. Pearson analysis, $^{*}P < 0.05$, $^{**}P < 0.01$, $^{***}P < 0.001$. The above 16S rRNA results were obtained from 4 mice in each group. (J) Growth curve of *Clostridium innocuum* treated with FLZ. $n = 5$ in each group. (K) The hydrolysis efficiency of GUDCA mediated by *Clostridium innocuum*. $n = 4$ in each group. Results are expressed as mean ± SEM. $^{*}P < 0.05$, $^{**}P < 0.01$, $^{***}P < 0.001$ *versus* Control mice; $^{\#}P < 0.05$, $^{\#\#}P < 0.01$, $^{\#\#\#}P < 0.001$ *versus* MPTP/p-treated mice.

Two-tailed unpaired Student's *t*-test and one-way ANOVA were used for comparisons of mouse and cell-related experiments, and a Kruskal−Wallis test was used for Simpson and Shannon analysis. Correlation analysis of gut microbiome and gut metabolites was performed using nonparametric Spearman's test. $P < 0.05$ was considered statistically significant.

3. Results

3.1. GUDCA was the main differential intestinal microbial metabolite in PD mice treated with FLZ

Consistent with previous studies, we found that FLZ was a safe and effective agent for PD treatment, as indicated by the increased body weight (Fig. S1C and S1D), improved motor coordination (Fig. S1E−S1H) and dopaminergic neuron function (Fig. S1I and S1J). FLZ alleviated gut dysfunction with increased intestinal movement (Supporting Information Fig. S2A−S2D) and decreased barrier permeability (Fig. S2E and S2F) in the MPTP/p induced PD mice, suggesting that FLZ might mitigate PD by improving intestinal function. Our previous study has confirmed that FLZ treatment could correct the gut microbiota dysbiosis, thus we performed untargeted metabolomics analysis and aimed to find out the critical gut microbiota metabolite altered by FLZ treatment, which was responsible for the alleviations of enteric dysfunction and motor disorder of PD mice. Distinct metabolic cluster in the midbrain, feces, plasma and urine was successfully formed among Control mice, MPTP/p-induced PD mice and FLZ-treated PD mice. FLZ had a tendency to restore the metabolic differentiation to the Control level as observed with closer distance between FLZ-treated group to Control group in the OPLS-DA analysis (Supporting Information Fig. S3A−S3D). The volcano plots also showed remarkable metabolite differences in fecal, urine, plasma, and midbrain samples among different groups (Fig. S3E−S3H). The Venn diagrams were drawn to observe the significantly affected metabolites. There were found 8 differential metabolites in the midbrain (Fig. 1A), 37 differential metabolites in the feces (Fig. 1B), 23 differential metabolites in the plasma (Fig. 1C) and 45 differential metabolites in the urine (Fig. 1D). We then compared the profiles of feces, urine and plasma to that of the midbrain, target tissue of PD. Two differential metabolites, GUDCA and (±)7(8)-DiHDPE(A) were identified (Fig. 1E). The two differential metabolites were significantly downregulated in the midbrain and feces of PD mice, which were then upregulated by FLZ treatment (Table 1). Among the top 20 differential metabolites with the most significantly altered FC value in the midbrain and fecal metabolic profiling, GUDCA was the most affected metabolites with the highest FC value in FLZ-treated PD mice (Fig. 1F and G). Moreover, GUDCA had the highest VIP value in the fecal and midbrain metabolic profiling and identified as top 20 differential metabolite with high FC value and high VIP value in the urine (Supporting Information Fig. S4). The ROC analysis, used for searching for PD biomarkers, showed that the AUC of GUDCA (0.792) was higher than that of (±)7(8)-DiHDPE(A) (0.722) in midbrain (Fig. 1H). Similarly, in the feces, the AUC of GUDCA (0.833) was also higher than that of (±)7(8)-DiHDPE(A) (0.722) (Fig. 1I). In addition, we calculated and compared the correlation coefficients of the two differential metabolites with PD pathological indexes, including latency of rotarod test, scores of pole test, fecal pellet output and fecal water content, respectively. Data showed that GUDCA was more related with these indexes than (±)7(8)-DiHDPE(A) due to the higher coefficient values (Fig. 1J). Finally, the assays of GUDCA concentrations in different tissues also illustrated that GUDCA was the most affected gut microbiota metabolite by FLZ treatment (Fig. 1K).

3.2. FLZ promoted GUDCA production through inhibiting BSH enzyme in Clostridium innocuum

Consistent with previous studies in rotenone-induced PD mice[15], our results based on alpha and beta diversity of 16S rRNA analysis showed that FLZ treatment could attenuate the MPTP/p-induced gut microbiota dysbiosis in PD mice (Fig. 2A−D). We then detailed analyzed the composition of gut flora and sought to identify which bacterium was responsible for the production of GUCDA. There were 9 differential microbiotas at phyla level detected in feces samples of PD mice, among which *Bacteroidota* and *Firmicutes* were dominant. FLZ treatment decreased the relative abundance of *Bacteroidota* and *Firmicutes* in MPTP/p-induced PD mice (Fig. 2E). The alternations at genus level analyzed by metastat delineated that the relative abundance of *Comamonas*, *Candidatus Saccharimonas*, and *Enterorhabdus* were markedly increased in PD mice after FLZ treatment. In contrast, the relative abundance of *Clostridium innocuum* which belongs to *Firmicutes* was significantly decreased after FLZ treatment compared with MPTP/p-induced PD mice (Fig. 2F and G). We next analyzed the correlations between GUDCA and the differential gut microbiota that identified above, and found that GUDCA was positively associated with *Candidatus Saccharimonas*, while negatively associated with *Clostridium innocuum* (Fig. 2H). Further correlation analysis between pathological indexes of PD and differential gut microbiota showed that *Clostridium innocuum* was more relevant to the pathological indexes than *Candidatu Saccharimonas* with higher correlation coefficient (Fig. 2I). The above results suggested that FLZ treatment increased the production of GUDCA might be through decreasing the relative abundance of *Clostridium innocuum.*

We then performed *in vitro* experiments to verify whether FLZ treatment can inhibit the growth of *Clostridium innocuum.* Data show that *Clostridium innocuum* growth was markedly inhibited after incubation with FLZ for 24 h (Fig. 2J). BSH enzyme is reported to be responsible for GUDCA deconjugation. In the liver, UDCA is conjugated to free-formed glycine *via* an amide bond, transferring into GUDCA. When GUDCA reaches the gut *via* enterohepatic circulation, BSH enzyme hydrolyzes this amide bond and catalyzes the deconjugation of GUDCA to ursodeoxycholic acid (UDCA). In this study, GUDCA was used as substrate for BSH enzyme in *Clostridium innocuum*, and the activity of BSH was reflected by GUDCA conversion efficiency. We employed riboflavin, a BSH enzyme inhibitor, to investigate whether BSH enzyme is present in *Clostridium innocuum* and in charge of GUDCA conversion by FLZ treatment. The results show that inhibition of BSH enzyme by riboflavin suppressed GUDCA conversion, indicating that *Clostridium innocuum* possesses BSH enzyme. FLZ significantly inhibited the conversion of GUDCA, confirming that FLZ treatment promoted GUDCA production by inhibiting the BSH enzyme in *Clostridium innocuum* (Fig. 2K).

3.3. GUDCA protected SH-SY5Y cells against the rotenone-induced apoptosis

As FLZ treatment upregulated GUDCA production, the main differential metabolite of *Clostridium innocuum* in PD mice, we employed the *in vitro* model of rotenone-challenged SH-SY5Y cells and sought to investigate whether GUDCA contributed to the

therapeutic effects of FLZ on PD. The results showed that 1 μmol/L of GUDCA increased the cell viability by 30.2% (Fig. 3A). Morphological observation showed that rotenone simulation led to cell shrinkage and membrane blebbing, but GUDCA treatment improved these morphological alterations (Fig. 3B). Moreover, rotenone stimulation caused significantly apoptosis of SH-SY5Y cell and as expected, flow cytometry showed that rotenone stimulation significantly increased the apoptosis of SH-SY5Y cell, but treatment with GUDCA (1 μmol/L) significantly inhibited apoptosis (Fig. 3C and D). GUDCA also decreased the expression levels of Bax

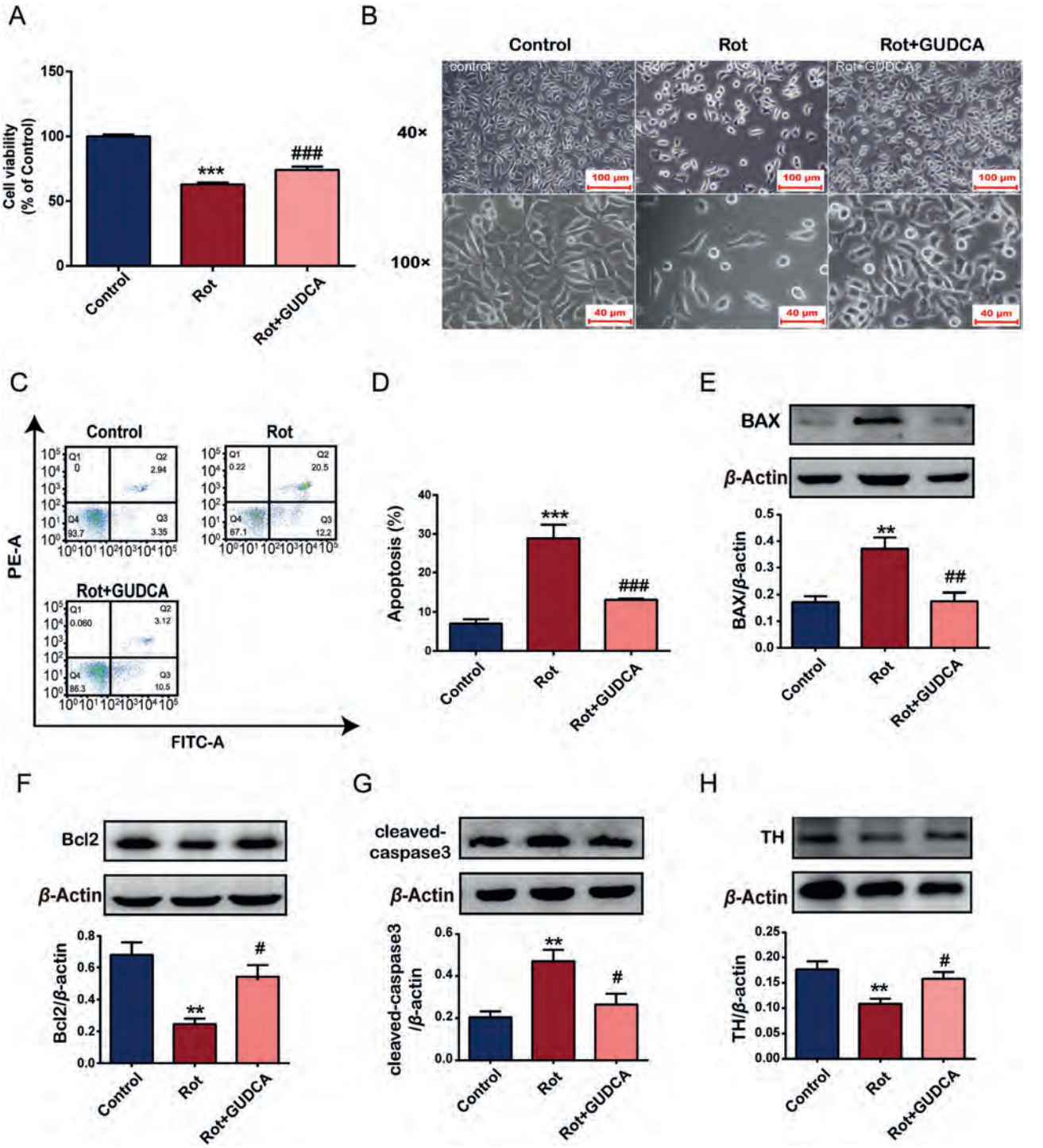

Figure 3 GUDCA protected SH-SY5Y cells against the rotenone-induced apoptosis. SH-SY5Y cells were stimulated with rotenone and treated GUDCA for 24 h. (A) Cell viability was measured by the CCK-8 assay, $n = 6-9$. (B) Cell morphology detected by phase-contrast micrographs. (C, D) representative of flow cytometry and quantitative analysis of apoptosis from three independent experiments. (E) Western blot analysis of Bax expression. (F) Western blot analysis of Bcl2 expression. (G) Western blot analysis of cleaved-caspase3 expression. (H) Western blot analysis of TH expression. Data are presented as mean ± SEM from 5 to 6 independent experiments. $^{*}P < 0.05$, $^{**}P < 0.01$, $^{***}P < 0.001$ *versus* Control cells; $^{\#}P < 0.05$, $^{\#\#}P < 0.01$, $^{\#\#\#}P < 0.001$ *versus* rotenone-stimulated cells.

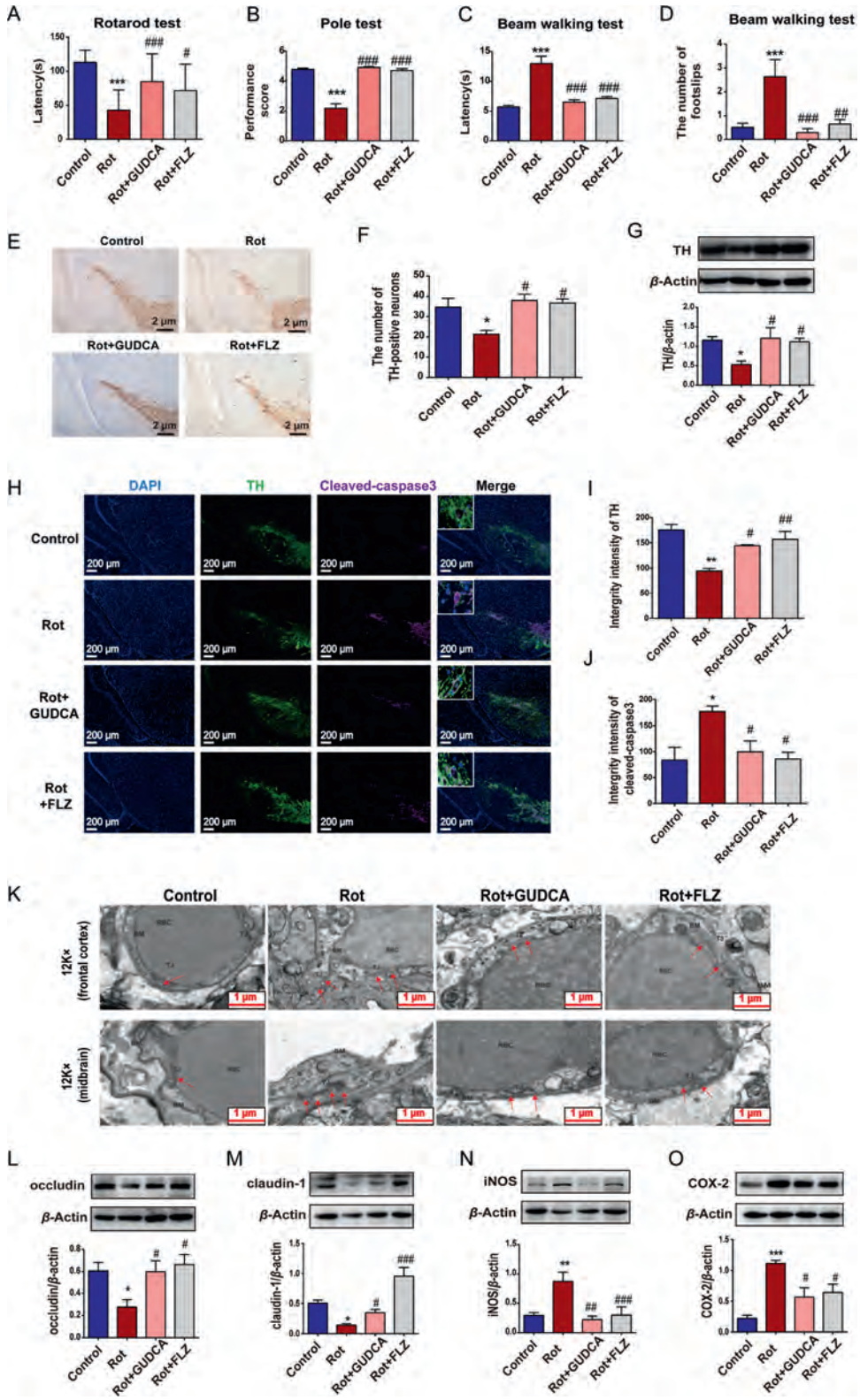

Figure 4 GUDCA improved motor coordination and brain tight junction function in rotenone-induced PD mice. The rotenone-induced PD mice were treated with GUDCA or FLZ for 4 weeks. The mice in each group were subjected to motor behavior tests, and then the midbrain, frontal cortex and striatum were collected at 6th week. (A) Rotarod tests. (B) Pole tests. (C) Latency in beam walking tests. (D) Number of footslips in beam walking tests. Behavior data were obtained from 11 to 16 mice. (E) Immunohistochemistry of TH staining in substantia nigra. Representative sections of the substantia nigra from three mice were shown. (F) Statistical analysis of TH positive cells. (G) Western blot analysis of TH expression in the striatum. (H) Co-staining of TH (green) and cleaved-caspase3 (purple) in substantia nigra, Scale bar: 200 μm. Representative sections were from three mice. (I, J) Statistical analysis of immunofluorescence intensities of TH and cleaved-caspase3. (I) Western blot

(Fig. 3E) and cleaved-caspase3 (Fig. 3G) and upregulated Bcl2 (Fig. 3F) in the rotenone-stimulated SH-SY5Y cells. TH level reflects dopaminergic neuron function, GUDCA treatment significantly increased TH protein expression (Fig. 3H). These data suggest that GUDCA can rescue dopaminergic neuron function against rotenone-induced neurotoxicity by attenuating apoptosis.

3.4. GUDCA improved motor coordination and brain barrier function in rotenone-induced PD mice

The neuroprotective effects of GUDCA were further verified in rotenone-induced PD mice by measuring motor behaviors and brain barrier functions. The results showed that GUDCA increased the duration of staying on the rod in the rotarod test (Fig. 4A), improved the performance in the pole test (Fig. 4B), decreased the time staying on the beam and the number of foot slips in the beam walking test (Fig. 4C and D). GUDCA also alleviated the pathological damages of the substantia nigra and striatum by increasing the number of TH positive neurons and TH expression, detected by immunohistochemistry analysis and Western blot, respectively (Fig. 4E−G). By co-staining cleaved-caspase3 with TH, we found that GUDCA markedly inhibited apoptosis of dopaminergic neurons in the substantia nigra (Fig. 4H−J). Tight junction is critical for the maintenance of the brain barrier permeability. As shown in Fig. 4K, the ultrastructures of tight junction in both the frontal cortex and midbrain were examined by TEM, showing that disorganized and diffuse structure, as well as remarkable local endothelial damage occurred in PD mice compared with the Control mice. GUDCA treatment remarkably improved the integrity and clarity of tight junction (red arrow) in the frontal cortex and midbrain of PD mice. Besides, damages of endothelial cells and surrounding brain tissues were also improved by GUDCA treatment (Fig. 4K). Next, we employed Western blot to detect the expression of occludin and claudin-1, the main tight junction proteins and found that GUDCA treatment could markedly increase the expression of these two proteins in the rotenone-induced PD mice (Fig. 4L and M). Previous studies have demonstrated that the tight junction impairment may cause neuroinflammation. Thus, we detected the expression of two major inflammation-related proteins, iNOS and COX-2, by Western blot in the midbrain of mice. GUDCA administration decreased the expression of the two inflammation-associated proteins, suggesting that GUDCA suppressed neuroinflammation (Fig. 4N and O). More importantly, the above neuroprotective effects of GUDCA on PD were equivalent to FLZ. These results demonstrated that the intestinal flora metabolite GUDCA had neuroprotective activity and mediated the therapeutic effects of FLZ on PD.

3.5. GUDCA improved intestinal function in rotenone-induced PD mice

Furthermore, the therapeutic effects of GUDCA on rotenone-induced gut dysfunction were also investigated. The results showed that GUDCA increased the fecal frequency (Fig. 5A) and fecal output in 1 h (Fig. 5B). As for the water content percentage of feces, the results showed no significant difference among groups (Fig. 5C). We then measured the colonic tight junction and inflammation, as gut barrier leakage and intestinal inflammation may cause the pro-inflammatory cytokines and pathogens influx into the circulation, trigger systemic inflammation and aggravates blood−brain barrier damage. As shown in Fig. 5D, the ultrastructure of tight junction examined by TEM showed shortened microvilli, irregular brush borders and wider intercellular gaps in PD mice compared with Control mice. GUDCA treatment remarkably improved the integrity and clarity of tight junctions (red arrow) (Fig. 5D). Next, we detected the expression of tight junction related proteins, occludin and claudin-1, and found that GUDCA treatment markedly increased the expression of these two proteins in the rotenone-induced PD mice (Fig. 5E and F). Western blot analysis of two major inflammation-related proteins, iNOS and COX-2, showed that GUDCA administration markedly decreased the expression of iNOS and COX-2, suggesting that GUDCA suppressed gut inflammation (Fig. 5G and H). Finally, we measured serum levels of inflammatory markers, including TNF-α and LPS. They were increased in the rotenone group when compared to Control group, while GUDCA treatment significantly decreased the level of TNF-α and LPS (Fig. 5I and J). It was worth noting that the above pharmacological effects of GUDCA on improving gut function were equivalent to FLZ. These results demonstrated that the GUDCA could alleviate gut dysfunction, systemic inflammation and contributed to the therapeutic effects of FLZ on improving gut function.

3.6. GUDCA alleviated PD pathological damage induced by rotenone through activating Nrf2 signaling pathway

GUDCA is an antagonist of FXR[22,23], and Nrf2, a potential upstream regulator of the cellular antioxidant system, can interact with FXR signaling pathway[24]. Thus, we focused on the FXR−Nrf2 signaling pathway to obtain further insights into the molecular mechanisms underlying the neuroprotective effects of GUDCA on dopaminergic neurons. Western blot analysis showed that the FXR expression was increased in SH-SY5Y cells exposed to rotenone, while GUDCA treatment significantly decreased its expression (Fig. 6A). The classical activation pattern of Nrf2 refers to its translocation from the cytoplasm to the nucleus. Hence, we then studied the nuclear translocation of Nrf2 in cells treated with GUDCA. The results indicated that Nrf2 expression in the whole cell lysates of rotenone-stimulated cells increased after treatment with GUDCA (Fig. 6B). In addition, the accumulation of Nrf2 in nucleus increased and the expression of Nrf2 in cytoplasm decreased when the cells were treated with GUDCA (Fig. 6C). The nuclear translocation of Nrf2 was also confirmed by immunofluorescence. In the rotenone-challenged cells, Nrf2 was mainly located in the cytoplasm, whereas Nrf2 translocated from the cytoplasm to the nucleus in the treatment of GUDCA (Fig. 6D). Moreover, both HO-1 and NQO1, two typical downstream factors of the Nrf2 pathway, were markedly upregulated in the treatment of GUDCA

analysis of occludin expression. (J) Western blot analysis of the claudin-1 expression. (K) Western blot analysis of the iNOS expression. (L) Western blot analysis of the COX-2 expression. (M) Western blot analysis of the claudin-1 expression. (N) Western blot analysis of the iNOS expression. (O) Western blot analysis of the COX-2 expression. The Western blot data were from 4 to 6 mice. Results are presented as mean ± SEM. $^{*}P < 0.05$, $^{**}P < 0.01$, $^{***}P < 0.001$ *versus* Control mice; $^{\#}P < 0.05$, $^{\#\#}P < 0.01$, $^{\#\#\#}P < 0.001$ *versus* rotenone-challenged mice.

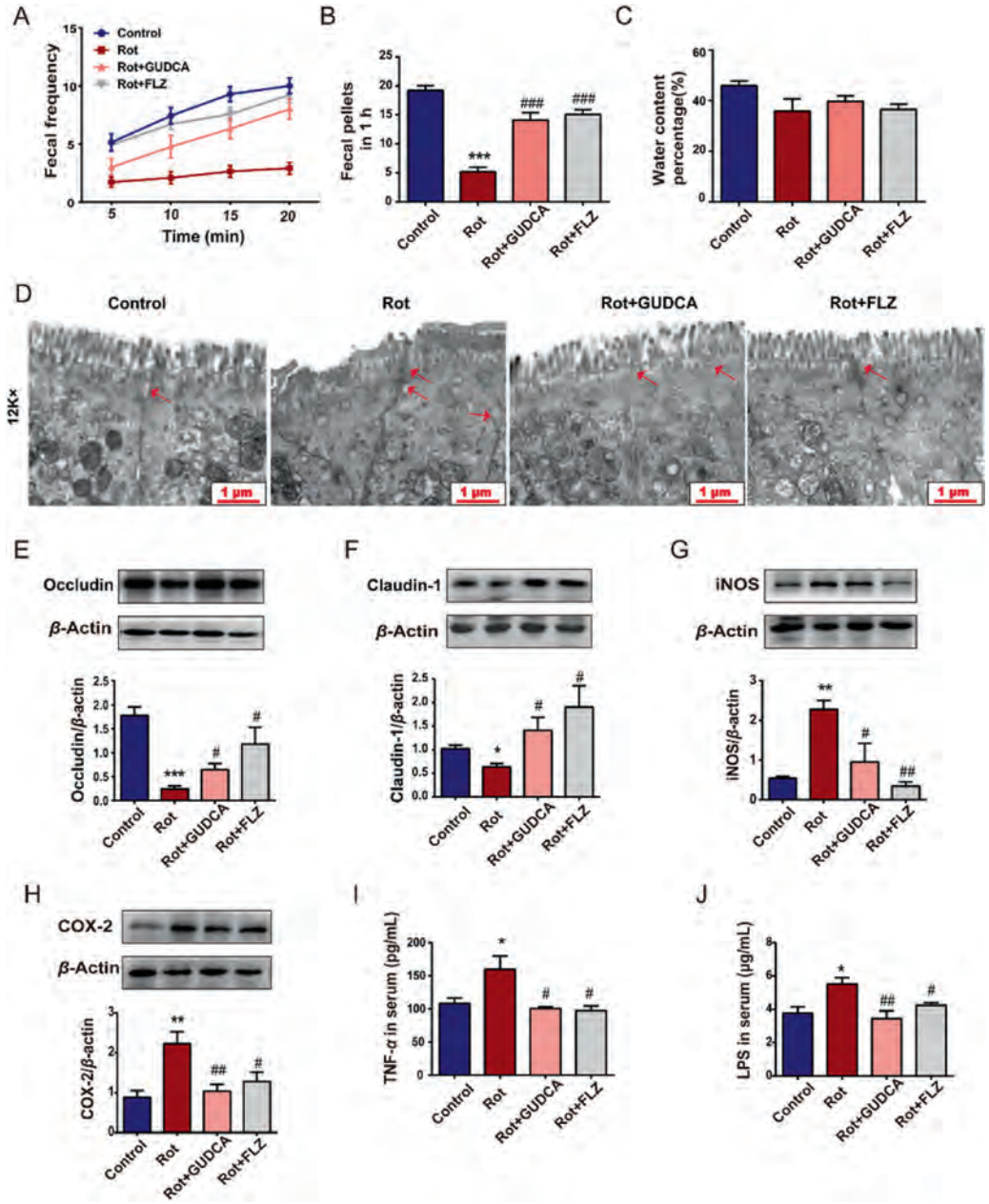

Figure 5 Effects of GUDCA on intestinal function and systemic inflammation in rotenone-induced PD mice model. The rotenone-induced PD mice were treated with GUDCA or FLZ for 4 weeks, and then the colon and fecal pellet were collected from 11 to 16 mice at 6th week. (A) Fecal frequency. (B) Fecal pellet output. (C) Fecal water content. (D) Representative electron micrographs showing the tight junction structure of gut barrier (red arrow). (E) Western blot analysis of occludin expression. (F) Western blot analysis of claudin-1 expression. (G)Western blot analysis of iNOS expression. (H) Western blot analysis of COX-2 expression. (I) Serum levels of TNF-α. (J) Serum levels of LPS. $n = 5$ in each group. Data are presented as mean ± SEM from 4 to 5 mice. $^{*}P < 0.05$, $^{**}P < 0.01$, $^{***}P < 0.005$ *versus* Control mice; $^{\#}P < 0.05$, $^{\#\#}P < 0.01$, $^{\#\#\#}P < 0.001$ *versus* rotenone-challenged mice.

(Fig. 6E and F), indicating that GUDCA facilitated Nrf2 nuclear translocation and then activated Nrf2 pathway. Consistent with the *in vitro* experiments, the same results were obtained from midbrains (Fig. 6G−K) and colons (Fig. 6L−P) in GUDCA-treated PD mice, showing that Nrf2 pathway was activated by GUDCA treatment. These *in vitro* and *in vivo* data clearly demonstrated that GUDCA, a metabolite produced from *Clostridium innocuum* by FLZ treatment, exerted neuroprotective effects on PD through activating Nrf2 signaling pathway.

4. Discussion

The microbiota−gut−brain axis is an intensive and extensive bidirectional communication between gut flora and CNS involving multiple pathways. Our previous studies have demonstrated that FLZ, a novel synthetic compound, exerting neuroprotective effects in several PD models[10-12]. In phase I clinical study, FLZ was well tolerated in healthy subjects with less side effects compared with current clinical medication. The beneficial effects of FLZ on PD

might be due to its anti-inflammatory activity, neuroprotection on dopaminergic neuron or influence on the composition of gut microbiota with multiple mechanisms[9,11,12]. Given the importance of microbial metabolites in regulation of microbiota-gut-brain axis, we conducted a set of experiments and explored the specific gut microbes and microbial metabolites that contribute to the therapeutical effects of FLZ on PD. Through metabolomics and 16S rRNA analysis, we identified GUDCA was the most affected differential microbial metabolite by FLZ treatment, and GUDCA was specially and negatively regulated by *Clostridium innocuum* through inhibiting the BSH enzyme. The protection of GUDCA on colon and CNS were confirmed in both *in vitro* and *in vivo* PD models through activating Nrf2 pathway, further validating that FLZ protected dopaminergic neurons through promoting GUDCA production (Fig. 7).

The GI tract provides one of the largest platforms for the communication between host and external environment. Within the GI tract, there is a complex ecological community consisting of 100 trillion microorganisms, named as the gut microbiota[25,26], which mainly maintains host homeostasis through regulating a wide range of pathophysiological functions. In recent years, the onset and development of PD was reported to be highly correlated with the gut microbiota dysbiosis. Increasing evidence showed that the composition and abundance of various intestinal bacteria are changed in PD, such as decreased *Akkermansia*, *Lactobacillus*, *Prevotella* and increased *Bifidobacterium*[27]. In our study remarkable changes in the intestinal flora of PD mice were also found, including decreased abundance of *Enterorhabdus, Candidatus Saccharimonas* and *Comamonas*, as well as increased abundance of *Clostridium innocuum* at the genus level of the PD mice, and FLZ treatment could correct these changes. Consistent with our pervious study[15], the abundance of *Enterorhabdus* was decreased in the PD mice, which was reported to be negatively related to inflammatory bowel disease (IBD), suggesting it has anti-inflammatory effect[28]. Due to a lack of information about *Enterorhabdus* in the development of PD, it is difficult to define the role of *Enterorhabdus* played in PD and more studies on *Enterorhabdus* were forcedly needed. Moreover, *Candidatus Saccharimonas* was observed to be related to inflammatory mucosal disease and regulated inflammation *via* decreasing *TNF-α* gene expression in macrophages[29]. In addition, low abundance of *Candidatus saccharimonas* was also detected in the both animal models of acute necrotizing pancreatitis and high-fat diet induced hypertriglyceridemia, which may also indicate the potential anti-inflammatory role of *Candidatus saccharimon*[29]. *Comamonas*, aerobic gram-negative bacteria, was reported to be abundant in late-onset PD patients[30]. On the contrary, our study indicated that the reduction in the abundance of *Comamonas* occurred in the PD mice. This discrepancy is possibly due to differences between PD patients and animal models. *Clostridium innocuum* is an anaerobic and gram-positive bacterium, which attracted much attention by its exclusive resistance to vancomycin[31]. As following, further studies found that high abundance of *Clostridium innocuum* was cytotoxic to gut epithelial cells[32], which probably contributed to extra-intestinal clostridial infection[33], a kind of severe gastrointestinal diseases with high mortality rate[33]. Moreover, recent studies indicated that *Clostridium innocuum* was highly correlated to diarrhoea[34] and tended to exacerbate IBD by inducing creeping fat[34,35], so *Clostridium innocuum* might be involved in PD development as IBD patients are susceptible to develop PD. In the present study, a high abundance of *Clostridium innocuum* in the gut was observed in PD mice by 16S rRNA analysis. Consistent with our results, a clinical study reported that the abundance of *Clostridium innocuum* was elevated in PD patients[36], indicating that *Clostridium innocuum* was critical in the pathogenesis of PD. When the PD mice were treated with FLZ, the abundance of *Clostridium innocuum* was markedly decreased, demonstrating that *Clostridium innocuum* might be the target bacterium of FLZ in treating PD.

Gut microbiota interacts with the host through their metabolites, forming an essential link between the gut microbiota and the host, which exerts vital and diverse effects on host physiology[37]. Many microbial metabolites are altered in PD patients and PD models, including SCFAs, vitaminB12, γ-aminobutyric acid, dopamine, tryptophan and secondary bile acid, etc. These microbial metabolites probably support the communication between microbiota and host *via* microbiota−gut−brain axis. For example, the SCFAs were reported to be decreased in the intestine of both PD patients[38] and PD mice[39], as well as improve PD motor behavior through alleviating the gut dysfunction[40]. Moreover, low level of microbial metabolite Vitamin B12 was observed in the serum of PD patients[41]. Vitamin B12 is mainly produced by *Lactobacillus*[42] and is associated with neuropathy and cognitive impairment[43]. In our study, various metabolites were significantly altered in the midbrain, feces, plasma and urine of PD mice after FLZ treatment. By comparing the levels of those altered differential metabolites in feces, plasma and urine to those in the midbrain, we preliminary identified two differential metabolites, GUDCA and (±)7(8)-DiHDPE(A). And then by comparing the FC value, ROC value, VIP value and calculating the correlation coefficient between above two differential metabolites and pathological indexes in PD, we targeted GUDCA as the differential metabolite that mediated the neuroprotection of FLZ on PD. In order to identify the differential microbiota that responsible for the conversion of GUDCA, we analyzed the correlation between GUDCA and the above mentioned four differential microbiotas. *Clostridium innocuum* had a higher correlation coefficient and pathological indexes relative to GUDCA. GUDCA is a glycine-conjugated form of UDCA and a major bile acid in the body with more hydrophilic and less toxic properties[44]. GUDCA is converted to UDCA in the gut by microbial BSH enzyme[45]. BSH enzyme regulates the first step of bile acid transformation in the gut. It is produced by the intestinal flora, especially highly expressed in the *Bifidobacterium* and *Lactobacillus* genus, which are strongly correlated to gut dysbiosis of PD. The bile salts including GUDCA derived from glycine are easily hydrolyzed by BSH enzyme compared with bile salts derived from taurine, such as tauroursodeoxycholic acid (TUDCA). In the present study, we employed the BSH enzyme inhibitor, riboflavin[46], and verified that the BSH enzyme was also presented in the *Clostridium innocuum.* As a result, the evidence suggests that the BSH enzyme is essential for the conversion of bile acid in PD. Moreover, we further observed that FLZ treatment could decrease the abundance of *Clostridium innocuum* and inhibit the BSH enzyme in the *Clostridium innocuum*, suggesting that FLZ treatment increased the production of GUDCA by inhibiting the BSH enzyme in the *Clostridium innocuum*. This is the first time to report that BSH enzyme was presented in the *Clostridium innocuum,* and is highly correlated to GUDCA production. Together, in FLZ-treated PD mice, we identified GUDCA was a significant differential metabolite, which achieved by specifically inhibiting BSH enzyme in the *Clostridium innocuum*.

GUDCA was reported to exert neuroprotective effects owing to its anti-apoptosis, anti-inflammatory and antioxidant properties. In the high levels of unconjugated bilirubin (UCB) induced rat

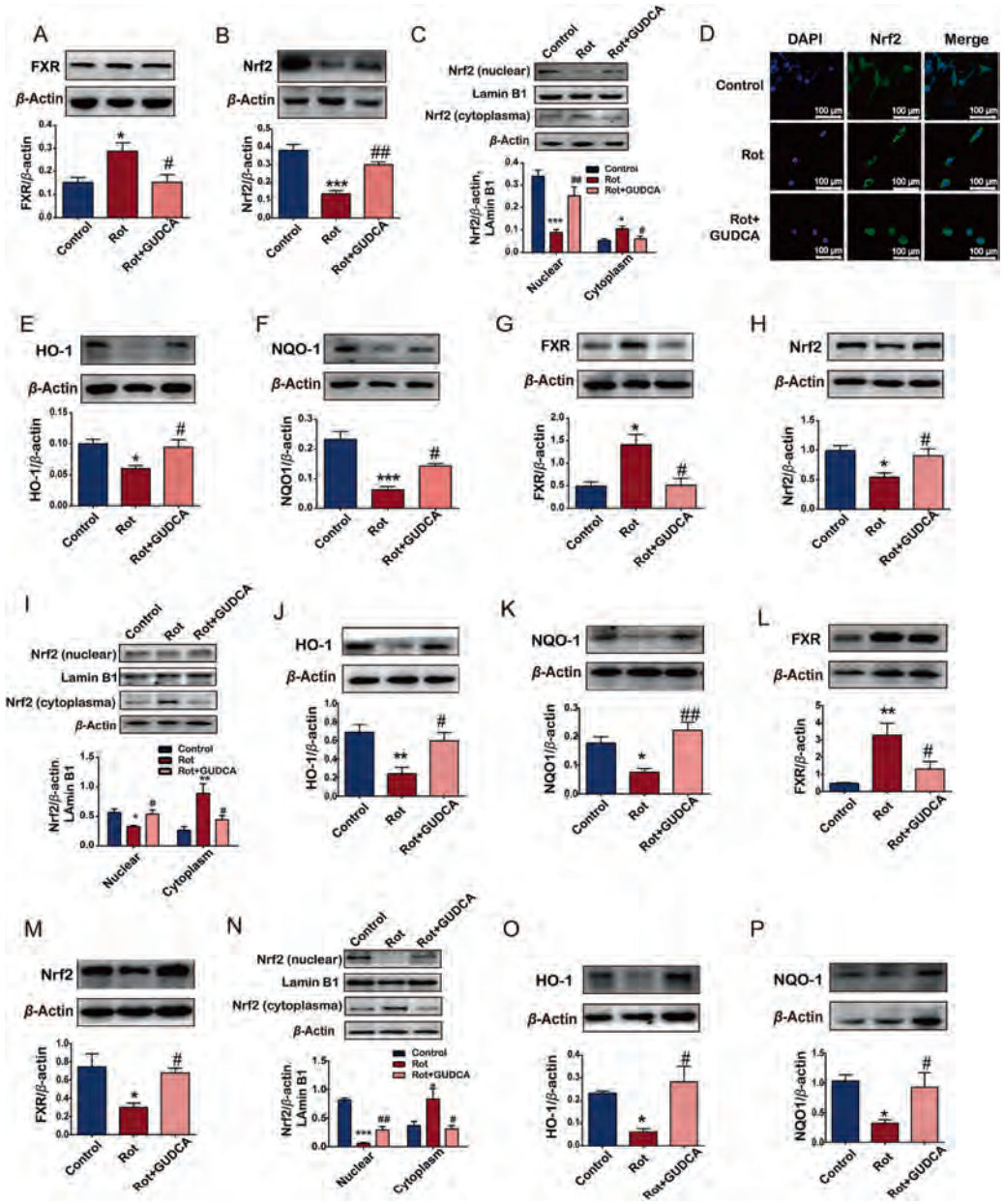

Figure 6 GUDCA alleviated neurotoxicity induced by rotenone through activating Nrf2 signaling pathway. SH-SY5Y cells were stimulated with rotenone and treated with GUDCA for 24 h. (A) Western blot analysis of FXR expression. (B) Western blot of the Nrf2 expression. (C) Western blot analysis of Nrf2 in the nucleus and cytoplasm. Data are presented as mean ± SEM from 4 to 6 independent experiment. (D) Confocal microscopy detection of Nrf2. Represent images of immunofluorescence were from four independent experiments. Scale bar:100 μm. (E) Western blot analysis of the HO-1. (F) Western blot analysis of NQO-1. Rotenone-induced PD mice were received FLZ and GUDCA treatments for 4 weeks, the midbrain and colon were then collected at 6th week. (G) Western blot analysis of FXR expression in the midbrain. (H) Western blot analysis of Nrf2 expression in the midbrain. (I) Western blot analysis of Nrf2 in the nucleus and cytoplasm of midbrain. (J) Western blot analysis of HO-1 expression in the midbrain. (K) Western blot analysis of NQO1 expression in the midbrain. (L) Western blot analysis of FXR expression in the colon. (M) Western blot analysis of Nrf2 expression in the colon. (N) Western blot analysis of Nrf2 in the nucleus and cytoplasm of colon. (O) Western blot analysis of HO-1 expression in the colon. (P) Western blot analysis of NQO1 expression in the colon. Data are presented as mean ± SEM from 4 to 6 independent experiments. $^{*}P < 0.05$, $^{**}P < 0.01$, $^{***}P < 0.001$ *versus* Control cells (mice); $^{\#}P < 0.05$, $^{\#\#}P < 0.01$, $^{\#\#\#}P < 0.001$ *versus* rotenone-challenged cells (mice).

cortical neuron apoptosis model, GUDCA prevented the neurons from apoptosis by attenuating UCB-induced cytochrome *c* oxidase inhibition and suppressing oxidative stress[47]. And in the UCB-induced astroglial inflammation model, GUDCA reduced the productions of TNF-α and IL-1β by inhibiting the converting enzyme[48]. Moreover, in the primary cultured neurons, GUDCA relieved the oxidative stress from inhibiting protein oxidation and lipid peroxidation in UCB induced the oxidative injury[49]. Besides, clinical studies have revealed that the concentration of GUDCA was decreased in the blood of PD patients[50,51]. These

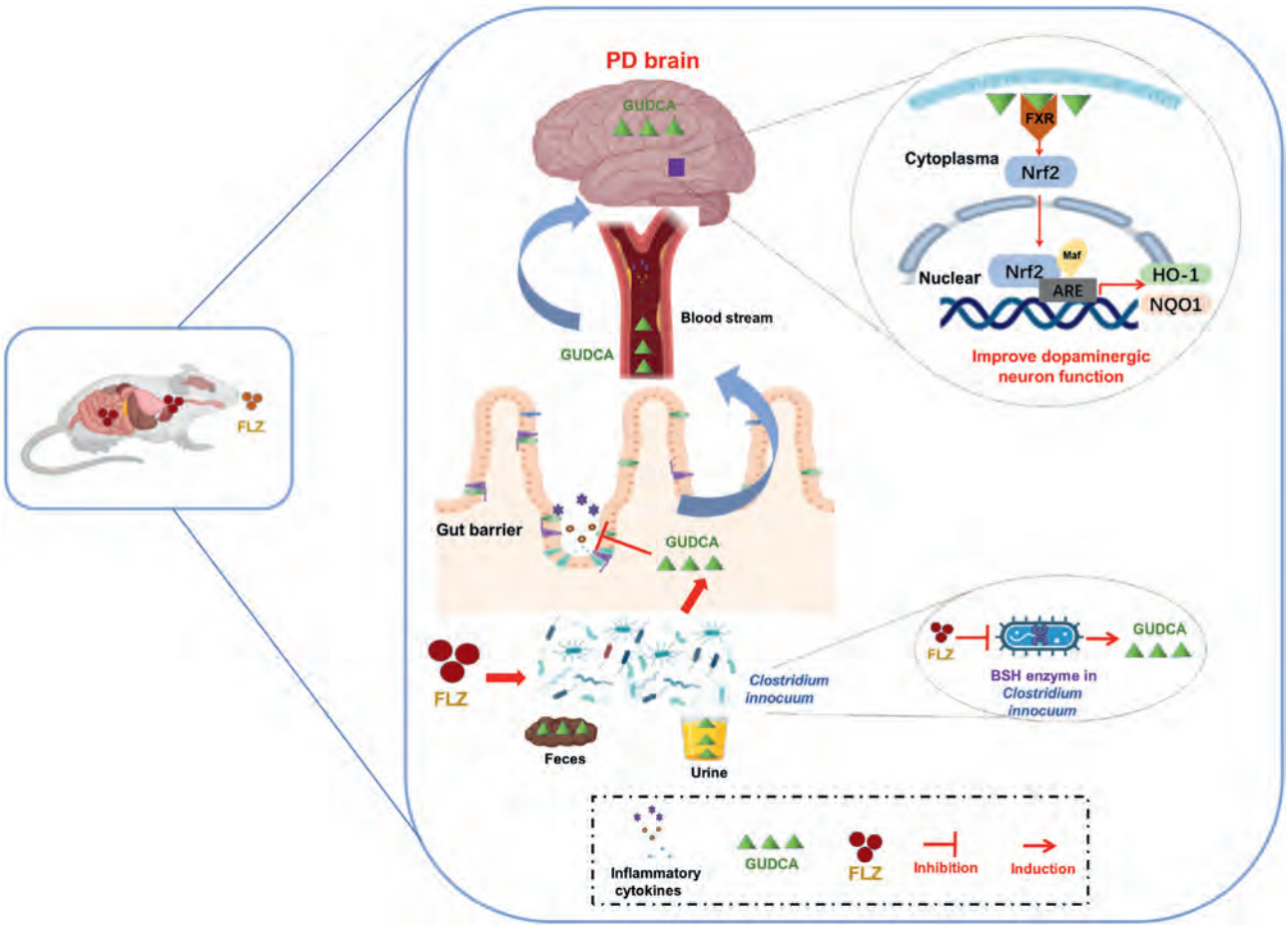

Figure 7 Schematic illustration of the proposed mechanisms by which FLZ alleviated PD pathological damage through increasing GUDCA production in *Clostridium innocuum*. In PD mouse model, FLZ treatment inhibited BSH enzyme activity in *Clostridium innocuum*, through which FLZ promoted the productions of GUDCA detected in the feces, urine, plasma and midbrain. The microbial metabolite GUDCA was capable of suppressing intestinal inflammation and therefore attenuated gut barrier destruction. As followed, GUDCA could improve systemic inflammation. GUDCA passed through blood−brain barrier, bound with FXR, and activated Nrf2 signaling pathway. Therefore, GUDCA suppressed neuroinflammation, restored brain barrier structure, and finally protected dopaminergic neurons from injury, further proving that regulation of the gut-brain axis is an important mechanism for FLZ to treat PD.

findings revealed that GUDCA is a promising neuroprotective agent and a potential biomarker of PD. These findings indicated that GUDCA is a promising neuroprotective agent. In the present study, we conducted *in vitro* and *in vivo* experiments in rotenone-induced PD models to further confirmed the neuroprotective effect of GUDCA. Consistent with previous studies, our result demonstrated that GUDCA could not only prevent apoptosis in rotenone-challenged SH-SY5Y cells, but also protect the dopaminergic neurons in the substantial nigra. Moreover, GUDCA was capable of attenuating neuroinflammation and brain barrier dysfunction and improving intestinal function in rotenone-induced PD mice, as indicated by decreasing inflammation, increasing tight junction of the gut as well. From our present results, we further found that GUDCA can play a protective role both in the central and peripheral nervous system. It was worth noting that the above neuroprotective effects of GUDCA on PD were equivalent to FLZ. We concluded that GUDCA produced by FLZ treatment could improve intestinal functions and decrease the systemic inflammation in PD mice, and finally alleviate the neuroinflammation, as well as improve dopaminergic neuron function, confirming that GUDCA could exert therapeutic effect on PD through regulating gut−brain axis. However, the neuroprotective effects of GUDCA require more extensive and in-depth study.

Furthermore, we investigated the molecular mechanism of GUDCA on improving PD. The GUDCA is an endogenous antagonist to FXR[24]. Recent studies reported that GUDCA binds to FXR and suppresses the interaction of FXR with retinoid X receptor a (RXRα) to inhibit the mTOR signaling pathway[52]. Moreover, FXR signaling has a mutual interaction with the Nrf2 signaling pathway. Several studies indicated that the suppression of FXR could lead to the activation of Nrf2 signaling pathway[53]. In contrast, the Nrf2 activation competes with FXR to regulate downstream signaling factors[24] and leads to the inhibition of FXR signaling pathway[23]. Nowadays, oxidative stress has been implicated as a major culprit in the pathogenesis of PD[54]. As a result, new therapeutic targets can be defined for reducing oxidative stress and neuronal damage[55]. The transcription factor nuclear factor Nrf2 is a central regulator of redox, metabolic, and protein homeostasis which interacting with many other signaling cascades[56], which is reported to be significant to regulate the

development of PD. Amount of evidence indicated that upregulating Nrf2 signaling pathway contributed to neuroprotective effect in both *in vitro* and *in vivo* PD models. Nrf2 activation can protect dopaminergic neurons against rotenone-induced apoptosis[57] and glial inflammation[58] by the reduction in oxidative stress. Nrf2 knockout mice displayed increased sensitivity to 6-OHDA or MPTP, and triggering Nrf2/ARE pathway by transplantation of astrocytes overexpressing Nrf2 could exert neuroprotective effect on 6-OHDA-induced mouse brain damage[59]. Moreover, Nrf2-knockout mice exhibited aggravated gliosis and dopaminergic degeneration in the MPTP mice model[60,61]. Interestingly, the TUDCA, a bile acid similar to GUDCA, has been found to be effective in treating PD[62]. By regulating the Nrf2 signaling pathway[63], TUDCA improved MPTP-induced dopaminergic neuron loss and dopamine transporter damage. Our present study also proved that by inhibiting FXR expression, GUDCA therefore facilitated the nuclear translocation of Nrf2 in PD models. HO-1 and NQO1, downstream factors of the Nrf2 pathway, are responsible for various forms of cellular outcomes and trigger cellular defensive effect on inflammation, oxidative stress or cytotoxicity induced neuronal injury[64-66]. HO-1 and NQO1 were markedly upregulated after the treatment with GUDCA. These data revealed that GUDCA protects the dopaminergic neuron against injury by activating Nrf2 signaling pathway.

5. Conclusions

Our results illustrated that FLZ enhanced GUDCA production by inhibiting the BSH enzyme in *Clostridium innocuum*, providing evidence for FLZ to treat PD, by which FLZ protected against PD *via* regulating the microbiota−gut−brain axis. Our data also highlighted that elucidating the pathophysiological role of the microbiota−gut−brain axis in PD can not only uncover the early pathogenesis of PD and predict the progression of neurodegeneration, but also develop the intestinal microbiome-oriented treatment strategies to maintain the homeostasis of the intestinal microenvironment with the possibility to slow the progression of PD.

Acknowledgments

This work was supported by The National Key Research and Development Program of China (grant No. 2023YFC3502800) and the CAMS Innovation Found for Medical Sciences (No. 2022-I2M-2-001, China).

Author contributions

Meiyu Shang: Writing − review & editing, Writing − original draft, Project administration, Formal analysis, Data curation, Conceptualization. Jingwen Ning: Project administration, Formal analysis. Caixia Zang: Data curation. Jingwei Ma: Project administration, Data curation. Yang Yang: Project administration, Data curation. Yueqi Jiang: Project administration, Conceptualization. Qiuzhu Chen: Project administration, Data curation. Yirong Dong: Project administration, Data curation. Jinrong Wang: Project administration, Data curation. Fangfang Li: Data curation. Xiuqi Bao: Supervision, Conceptualization. Dan Zhang: Supervision, Conceptualization.

Conflicts of interest

The authors declare that they have no competing interests.

Appendix A. Supporting information

Supporting information to this article can be found online at https://doi.org/10.1016/j.apsb.2024.10.011.

References

1. Bloem BR, Okun MS, Klein C. Parkinson's disease. *Lancet* 2021;**397**:2284−303.
2. Pfeiffer RF. Gastrointestinal dysfunction in Parkinson's disease. *Lancet Neurol* 2003;**2**:107−16.
3. Pfeiffer RF. Gastrointestinal dysfunction in Parkinson's disease. *Parkinsonism Relat Disord* 2011;**17**:10−5.
4. Holmqvist S, Chutna O, Bousset L, Aldrin-Kirk P, Li W, Björklund T, et al. Direct evidence of Parkinson pathology spread from the gastrointestinal tract to the brain in rats. *Acta Neuropathol* 2014;**128**:805−20.
5. Chen ZJ, Liang CY, Yang LQ, Ren SM, Xia YM, Cui L, et al. Association of Parkinson's disease with microbes and microbiological therapy. *Front Cell Infect Microbiol* 2021;**11**:619354.
6. Agus A, Clément K, Sokol H. Gut microbiota-derived metabolites as central regulators in metabolic disorders. *Gut* 2021;**70**:1174−82.
7. Zhao Z, Ning J, Bao XQ, Shang M, Ma J, Li G, et al. Fecal microbiota transplantation protects rotenone-induced Parkinson's disease mice *via* suppressing inflammation mediated by the lipopolysaccharide−TLR4 signaling pathway through the microbiota−gut−brain axis. *Microbiome* 2021;**9**:1−27.
8. Huan P, Wang L, He Z, He J. The role of gut microbiota in the progression of Parkinson's disease and the mechanism of intervention by traditional Chinese medicine. *Neuropsychiatr Dis Treat* 2022;**18**:1507−20.
9. Bao XQ, Kong XC, Qian C, Zhang D. FLZ protects dopaminergic neuron through activating protein kinase B/mammalian target of rapamycin pathway and inhibiting RTP801 expression in Parkinson's disease models. *Neuroscience* 2012;**202**:396−404.
10. Bao XQ, Kong XC, Kong LB, Wu LY, Sun H, Zhang D. Squamosamide derivative FLZ protected dopaminergic neuron by activating Akt signaling pathway in 6-OHDA-induced *in vivo* and *in vitro* Parkinson's disease models. *Brain Res* 2014;**1547**:49−57.
11. Bao XQ, Wu LY, Wang XL, Sun H, Zhang D. Squamosamide derivative FLZ protected tyrosine hydroxylase function in a chronic MPTP/probenecid mouse model of Parkinson's disease. *Naunyn Schmiedebergs Arch Pharmacol* 2015;**388**:549−56.
12. Bao XQ, Wang XL, Zhang D. FLZ attenuates α-synuclein-induced neurotoxicity by activating heat shock protein 70. *Mol Neurobiol* 2017;**54**:349−61.
13. Tai W, Ye X, Bao X, Zhao B, Wang X, Zhang D. Inhibition of Src tyrosine kinase activity by squamosamide derivative FLZ attenuates neuroinflammation in both *in vivo* and *in vitro* Parkinson's disease models. *Neuropharmacology* 2013;**75**:201−12.
14. Shang J, Ma S, Zang C, Bao X, Wang Y, Zhang D. Gut microbiota mediates the absorption of FLZ, a new drug for Parkinson's disease treatment. *Acta Pharm Sin B* 2021;**11**:1213−26.
15. Zhao Z, Li F, Ning J, Peng R, Shang J, Liu H, et al. Novel compound FLZ alleviates rotenone-induced PD mouse model by suppressing TLR4/MyD88/NF-κB pathway through microbiota−gut−brain axis. *Acta Pharm Sin B* 2021;**11**:2859−79.
16. Magoč T, Salzberg SL. FLASH: fast length adjustment of short reads to improve genome assemblies. *Bioinformatics* 2011;**27**:2957−63.
17. Bokulich NA, Subramanian S, Faith JJ, Gevers D, Gordon JI, Knight R, et al. Quality-filtering vastly improves diversity estimates from Illumina amplicon sequencing. *Nat Methods* 2013;**10**:57−9.

18. Caporaso JG, Kuczynski J, Stombaugh J, Bittinger K, Bushman FD, Costello EK, et al. QIIME allows analysis of high-throughput community sequencing data. *Nat Methods* 2010;**7**:335−6.
19. Edgar RC, Haas BJ, Clemente JC, Quince C, Knight R. UCHIME improves sensitivity and speed of chimera detection. *Bioinformatics* 2011;**27**:2194−200.
20. Haas BJ, Gevers D, Earl AM, Feldgarden M, Ward DV, Giannoukos G, et al. Chimeric 16S rRNA sequence formation and detection in Sanger and 454-pyrosequenced PCR amplicons. *Genome Res* 2011;**21**: 494−504.
21. Zhao Z, Bao XQ, Zhang Z, Liu H, Zhang D. Phloroglucinol derivative compound 21 attenuates cuprizone-induced multiple sclerosis mice through promoting remyelination and inhibiting neuroinflammation. *Sci China Life Sci* 2020;**63**:905−14.
22. Lu C, Zhang F, Xu W, Wu X, Lian N, Jin H, et al. Curcumin attenuates ethanol-induced hepatic steatosis through modulating Nrf2/FXR signaling in hepatocytes. *IUBMB Life* 2015;**67**:645−58.
23. Kim EY, Lee JM. NRF2 activation in autophagy defects suppresses a pharmacological transactivation of the nuclear receptor FXR. *Antioxidants* 2022;**11**:370.
24. Kay HY, Kim WD, Hwang SJ, Choi HS, Gilroy RK, Wan YJ, et al. Nrf2 inhibits LXRα-dependent hepatic lipogenesis by competing with FXR for acetylase binding. *Antioxid Redox Signal* 2011;**15**:2135−46.
25. Thursby E, Juge N. Introduction to the human gut microbiota. *Biochem J* 2017;**474**:1823−36.
26. Rinninella E, Raoul P, Cintoni M, Franceschi F, Miggiano GAD, Gasbarrini A, et al. What is the healthy gut microbiota composition? A changing ecosystem across age, environment, diet, and diseases. *Microorganisms* 2019;**7**:14.
27. Gerhardt S, Mohajeri MH. Changes of colonic bacterial composition in Parkinson's disease and other neurodegenerative diseases. *Nutrients* 2018;**10**:708.
28. Liu B, Ye D, Yang H, Song J, Sun X, Mao Y, et al. Two-sample mendelian randomization analysis investigates causal associations between gut microbial genera and inflammatory bowel disease, and specificity causal associations in ulcerative colitis or Crohn's disease. *Front Immunol* 2022;**13**:921546.
29. Gryaznova M, Dvoretskaya Y, Burakova I, Syromyatnikov M, Popov E, Kokina A, et al. Dynamics of changes in the gut microbiota of healthy mice fed with lactic acid bacteria and bifidobacteria. *Microorganisms* 2022;**10**:1020.
30. Lin A, Zheng W, He Y, Tang W, Wei X, He R, et al. Gut microbiota in patients with Parkinson's disease in southern China. *Parkinsonism Relat Disord* 2018;**53**:82−8.
31. Chia JH, Feng Y, Su LH, Wu TL, Chen CL, Liang YH, et al. *Clostridium innocuum* is a significant vancomycin-resistant pathogen for extra-intestinal clostridial infection. *Clin Microbiol Infect* 2017;**23**:560−6.
32. Wu HY, Kuo CJ, Chou CH, Ho MW, Chen CL, Hsu TS, et al. *Clostridium innocuum*, an emerging pathogen that induces lipid raft-mediated cytotoxicity. *Virulence* 2023;**14**:2265048.
33. Cherny KE, Muscat EB, Reyna ME, Kociolek LK. *Clostridium innocuum*: microbiological and clinical characteristics of a potential emerging pathogen. *Anaerobe* 2021;**71**:102418.
34. Le PH, Chiu CT, Yeh PJ, Pan YB, Chiu CH. *Clostridium innocuum* infection in hospitalised patients with inflammatory bowel disease. *J Infect* 2022;**84**:337−42.
35. Dickson I. Creeping fat in Crohn's disease explained. *Nat Rev Gastroenterol Hepatol* 2020;**17**:713.
36. Nishiwaki H, Ito M, Ishida T, Hamaguchi T, Maeda T, Kashihara K, et al. Meta-analysis of gut dysbiosis in Parkinson's disease. *Mov Disord* 2020;**35**:1626−35.
37. Lavelle A, Sokol H. Gut microbiota-derived metabolites as key actors in inflammatory bowel disease. *Nat Rev Gastroenterol Hepatol* 2020; **17**:223−37.
38. Aho VT, Houser MC, Pereira PA, Chang J, Rudi K, Paulin L, et al. Relationships of gut microbiota, short-chain fatty acids, inflammation, and the gut barrier in Parkinson's disease. *Mol Neurodegener* 2021;**16**:1−14.
39. Hou Y, Li X, Liu C, Zhang M, Zhang X, Ge S, et al. Neuroprotective effects of short-chain fatty acids in MPTP induced mice model of Parkinson's disease. *Exp Gerontol* 2021;**150**:111376.
40. Shin C, Lim Y, Lim H, Ahn TB. Plasma short-chain fatty acids in patients with Parkinson's disease. *Mov Disord* 2020;**35**:1021−7.
41. Christine CW, Auinger P, Joslin A, Yelpaala Y, Green R, Investigators PSGD. Vitamin B12 and homocysteine levels predict different outcomes in early Parkinson's disease. *Mov Disord* 2018;**33**:762−70.
42. Santos F, Teusink B, Molenaar D, van Heck M, Wels M, Sieuwerts S, et al. Effect of amino acid availability on vitamin B12 production in *Lactobacillus reuteri*. *Appl Environ Microbiol* 2009;**75**:3930−6.
43. Moore E, Mander A, Ames D, Carne R, Sanders K, Watters D. Cognitive impairment and vitamin B12: a review. *Int Psychogeriatr* 2012;**24**:541−56.
44. Wunsch E, Trottier J, Milkiewicz M, Raszeja-Wyszomirska J, Hirschfield GM, Barbier O, et al. Prospective evaluation of ursodeoxycholic acid withdrawal in patients with primary sclerosing cholangitis. *Hepatology* 2014;**60**:931−40.
45. Li C, Ji Q, He T, Liu Y, Ma Y. Characterization of a recombinant bile salt hydrolase (BSH) from *Bifidobacterium bifidum* for its glycine-conjugated bile salts specificity. *Biocatal Biotransform* 2021;**39**:61−70.
46. Lin J, Negga R, Zeng X, Smith K. Effect of bile salt hydrolase inhibitors on a bile salt hydrolase from *Lactobacillus acidophilus*. *Pathogens* 2014;**3**:947−56.
47. Vaz AR, Delgado-Esteban M, Brito MA, Bolaños JP, Brites D, Almeida A. Bilirubin selectively inhibits cytochrome *c* oxidase activity and induces apoptosis in immature cortical neurons: assessment of the protective effects of glycoursodeoxycholic acid. *J Neurochem* 2010;**112**:56−65.
48. Fernandes A, Vaz AR, Falcao AS, Silva RF, Brito MA, Brites D. Glycoursodeoxycholic acid and interleukin-10 modulate the reactivity of rat cortical astrocytes to unconjugated bilirubin. *J Neuropathol Exp Neurol* 2007;**66**:789−98.
49. Brito MA, Lima S, Fernandes A, Falcao AS, Silva RF, Butterfield DA, et al. Bilirubin injury to neurons: contribution of oxidative stress and rescue by glycoursodeoxycholic acid. *Neurotoxicology* 2008;**29**:259−69.
50. Zhao H, Wang C, Zhao N, Li W, Yang Z, Liu X, et al. Potential biomarkers of Parkinson's disease revealed by plasma metabolic profiling. *J Chromatogr B* 2018;**1081**:101−8.
51. Shao Y, Li T, Liu Z, Wang X, Xu X, Li S, et al. Comprehensive metabolic profiling of Parkinson's disease by liquid chromatography-mass spectrometry. *Mol Neurodegener* 2021;**16**:1−15.
52. Zeng D, Zhang L, Luo Q. Celastrol-regulated gut microbiota and bile acid metabolism alleviate hepatocellular carcinoma proliferation by regulating the interaction between FXR and RXRα *in vivo* and *in vitro*. *Front Pharmacol* 2023;**14**:1124240.
53. Yan M, Guo L, Ma J, Yang Y, Tang T, Zhang B, et al. Liquiritin alleviates alpha-naphthylisothiocyanate-induced intrahepatic cholestasis through the Sirt1/FXR/Nrf2 pathway. *J Appl Toxicol* 2023;**43**:350−9.
54. Feng J, Zheng Y, Guo M, Ares I, Martínez M, Lopez-Torres B, et al. Oxidative stress, the blood−brain barrier and neurodegenerative diseases: the critical beneficial role of dietary antioxidants. *Acta Pharm Sin B* 2023;**13**:3988−4024.
55. Cuadrado A, Moreno-Murciano P, Pedraza-Chaverri J. The transcription factor Nrf2 as a new therapeutic target in Parkinson's disease. *Expert Opin Ther Targets* 2009;**13**:319−29.
56. Dodson M, de la Vega MR, Cholanians AB, Schmidlin CJ, Chapman E, Zhang DD. Modulating NRF2 in disease: timing is everything. *Ann Rev Pharmacol Toxicol* 2019;**59**:555−75.
57. Wei YZ, Zhu GF, Zheng CQ, Li JJ, Sheng S, Li DD, et al. Ellagic acid protects dopamine neurons from rotenone-induced neurotoxicity *via* activation of Nrf2 signalling. *J Cell Mol Med* 2020;**24**:9446−56.
58. Sun W, Li H, Shen Y, Xiao H. Resveratrol attenuates rotenone-induced inflammation and oxidative stress *via* STAT1 and Nrf2/Keap1/SLC7A11 pathway in a microglia cell line. *Pathol Res Pract* 2021;**225**:153576.
59. Jakel RJ, Townsend JA, Kraft AD, Johnson JA. Nrf2-mediated protection against 6-hydroxydopamine. *Brain Res* 2007;**1144**:192−201.

60. Marro S, Chiabrando D, Messana E, Stolte J, Turco E, Tolosano E, et al. Heme controls ferroportin1 (FPN1) transcription involving Bach1, Nrf2 and a MARE/ARE sequence motif at position-7007 of the FPN1 promoter. *Haematologica* 2010;**95**:1261.
61. Pietsch EC, Chan JY, Torti FM, Torti SV. Nrf2 mediates the induction of ferritin H in response to xenobiotics and cancer chemopreventive dithiolethiones. *J Biol Chem* 2003;**278**:2361−9.
62. Cuevas E, Burks S, Raymick J, Robinson B, Gómez-Crisóstomo NP, Escudero-Lourdes C, et al. Tauroursodeoxycholic acid (TUDCA) is neuroprotective in a chronic mouse model of Parkinson's disease. *Nutr Neurosci* 2022;**25**:1374−91.
63. Moreira S, Fonseca I, Nunes MJ, Rosa A, Lemos L, Rodrigues E, et al. Nrf2 activation by tauroursodeoxycholic acid in experimental models of Parkinson's disease. *Exp Neurol* 2017;**295**:77−87.
64. Keum YS, Han YH, Liew C, Kim JH, Xu C, Yuan X, et al. Induction of heme oxygenase-1 (HO-1) and NAD[P]H:quinone oxidoreductase 1 (NQO1) by a phenolic antioxidant, butylated hydroxyanisole (BHA) and its metabolite, *tert*-butylhydroquinone (tBHQ) in primary-cultured human and rat hepatocytes. *Pharm Res (N Y)* 2006;**23**:2586−94.
65. Park JE, Park JS, Leem YH, Kim DY, Kim HS. NQO1 mediates the anti-inflammatory effects of nootkatone in lipopolysaccharide-induced neuroinflammation by modulating the AMPK signaling pathway. *Free Radic Biol Med* 2021;**164**:354−68.
66. He J, Zhou D, Yan B. Eriocitrin alleviates oxidative stress and inflammatory response in cerebral ischemia reperfusion rats by regulating phosphorylation levels of Nrf2/NQO-1/HO-1/NF-κB p65 proteins. *Ann Transl Med* 2020;**8**:757.